

Coastal polynyas in the southern Weddell Sea: Variability of the surface energy budget

Ian A. Renfrew and John C. King

British Antarctic Survey, Cambridge, UK

Thorsten Markus

NASA Goddard Space Flight Center, Greenbelt, Maryland, USA

Received 16 November 2000; revised 13 August 2001; accepted 26 September 2001; published 28 June 2002.

[1] The surface energy budget of coastal polynyas in the southern Weddell Sea has been evaluated for the period 1992–1998 using a combination of satellite observations, meteorological data, and simple physical models. The study focuses on polynyas that habitually form off the Ronne Ice Shelf. The coastal polynya areal data are derived from an advanced multichannel polynya detection algorithm applied to passive microwave brightness temperatures. The surface sensible and latent heat fluxes are calculated via a fetch-dependent model of the convective-thermal internal boundary layer. The radiative fluxes are calculated using well-established empirical formulae and an innovative cloud model. Standard meteorological variables that are required for the flux calculations are taken from automatic weather stations and from the National Centers for Environmental Production/National Center for Atmospheric Research reanalyses. The 7 year surface energy budget shows an overall oceanic warming due to the presence of coastal polynyas. For most of the period the summertime oceanic warming, due to the absorption of shortwave radiation, is approximately in balance with the wintertime oceanic cooling. However, the anomalously large summertime polynya of 1997–1998 allowed a large oceanic warming of the region. Wintertime freezing seasons are characterized by episodes of high heat fluxes interspersed with more quiescent periods and controlled by coastal polynya dynamics. The high heat fluxes are primarily due to the sensible heat flux component, with smaller complementary latent and radiative flux components. The average freezing season area-integrated energy exchange is 3.48×10^{19} J, with contributions of 63, 22, and 15% from the sensible, latent, and radiative components, respectively. The average melting season area-integrated energy exchange is -5.31×10^{19} J, almost entirely due to the radiative component. There is considerable interannual variability in the surface energy budget. The standard deviation of the energy exchange during the freezing (melting) season is 28% (95%) of the mean. During the freezing season, positive surface heat fluxes are equated with ice production rates. The average annual coastal polynya ice production is 1.11×10^{11} m³ (or 24 m per unit area), with a range from 0.71×10^{11} (in 1994) to 1.55×10^{11} m³ (in 1995). This can be compared to the estimated total ice production for the entire Weddell Sea: on average the coastal polynya ice production makes up 6.08% of the total, with a range from 3.65 (in 1994) to 9.11% (in 1995). *INDEX TERMS:* 3349 Meteorology and Atmospheric Dynamics: Polar meteorology; 4540 Oceanography: Physical: Ice mechanics and air/sea/ice exchange processes; 4207 Oceanography: General: Arctic and Antarctic oceanography; 4504 Oceanography: Physical: Air/sea interactions (0312); *KEYWORDS:* polynyas, sea ice, Weddell Sea, surface energy budget, surface fluxes, high-salinity shelf water

1. Introduction

[2] Coastal polynyas are regions of open water, or thin ice, formed by offshore winds blowing the sea ice pack out to sea. Their fixed locations provide a focus for wintertime air-sea-ice interactions within the polar regions, as the

exposure of belts of relatively warm water to the cold polar atmosphere allows the exchange of vast quantities of heat, cooling the surface ocean and warming the boundary layer of the atmosphere. If the ocean is at freezing point, the cooling results directly in ice production; hence there is a release of latent heat and a rejection of salt as ice is formed. The rejected salt-enriched brine acts as a positive density forcing [e.g., *Curry and Webster, 1999*]. The atmospheric warming leads to changes in boundary layer dynamics, for

example, the generation of convective plumes and, in general, an increase in boundary layer winds due to downward momentum transport [e.g., *Dare and Atkinson*, 1999]. The latent heat of fusion released as ice forms within wind-generated polynyas means they are often referred to as “latent heat” polynyas [e.g., *Smith et al.*, 1990].

[3] The impact of coastal polynyas on the ocean is important for several reasons. The fixed location, tied to the coastline and in regions prone to strong wind forcing, means the density forcing of the ocean is also spatially fixed. Indeed, as the air-sea exchange within a polynya is 1 or 2 orders of magnitude greater than through the surrounding sea ice, the local ocean forcing is likely to be dominated by the coastal polynya contribution. In this study we focus on the coastal polynyas that habitually form off the Ronne Ice Shelf, in the southern Weddell Sea (Figure 1). This is an important region oceanographically as it is in the Weddell Sea that the major portion of Antarctic Bottom Water (the most extensive water mass in the world ocean) is thought to be generated through a number of pathways [e.g., *Foldvik and Gammelsrød*, 1988]. Most of the pathways have as a starting point High Salinity Shelf Water, a dense water mass formed by salinization of Circumpolar Deep Water over the continental shelf. The salinization is caused by the production of sea ice, and as coastal polynyas tend to be located over the continental shelves, they are thought to be the primary production sites of High Salinity Shelf Water. Previous studies have shown the Ronne-Flichner Ice Shelf to be the most active area of the Weddell Sea for coastal polynyas [*Markus et al.*, 1998; *Comsio and Gordon*, 1998], so we concentrate on this region. An additional motivation for the work is to help in the interpretation and modeling of the oceanography beneath Ronne Ice Shelf [e.g., *Nicholls and Makinson*, 1998].

[4] In this paper we present a climatology of the surface energy budget within coastal polynyas off the Ronne Ice Shelf between 1992 and 1998. The surface energy budget can be written as

$$Q_s + Q_l + Q_r + Q_p + Q_o = Q_{\text{tot}} = \rho_i L_f F, \quad (1)$$

where Q_s is the sensible heat flux, Q_l is the latent heat flux, Q_r is the net radiative heat flux, Q_p is the heat flux from precipitation, Q_o is the upward heatflux from the ocean, and Q_{tot} is the total heat flux [e.g., *Curry and Webster*, 1999]. We take the sign convention that fluxes from the ocean to the atmosphere are positive. If the ocean is at freezing point, the total heat flux can be equated with an ice production rate F , where ρ_i is the density of ice and L_f is the latent heat of fusion. The Q_p flux can be significant if the precipitation falls as snow and so draws heat from the ocean as it melts [e.g., *Moore et al.*, 2002]. However, the amount of precipitation thought to fall within these Antarctic polynyas is not large, and so, we neglect this term. The upward oceanic heat flux Q_o is of the order 10 W m^{-2} for the Antarctic sea ice zone [*McPhee and Martinson*, 1994], which is small compared to the other terms; hence we also neglect this component of the surface energy budget.

[5] To develop this climatology, a number of data sets and models have been blended to provide a comprehensive treatment of the atmosphere-ocean-ice system. Our philosophy has been to use observational data wherever possible.



Figure 1. A map of the southern Weddell Sea region. The study region is marked by the inner rectangle.

Hence, to determine polynya areas over the period, we use passive microwave satellite observations and an advanced multichannel polynya detection algorithm first presented by *Markus and Burns* [1995]. This data set dictates our choice of the 1992–1998 time period.

[6] Direct observations of components of the surface energy budget within polynyas are rare and, if they do exist, only cover short experimental periods such as scientific cruises. Hence other data sources must be used, for example, observations from automatic weather stations (AWS) positioned on the edge of the ice shelf, generally just upwind of the coastal polynya. Unfortunately, the AWS data for the Ronne Ice Shelf do not cover the full 7 year period of our climatology, and so, we have chosen to use boundary layer data extracted from numerical weather prediction (NWP) model analyses and check this data set against the AWS data to obtain an estimate of its accuracy. Both a 1 year AWS climatology and a 7 year model climatology are calculated. The atmospheric boundary layer immediately over an ice shelf and that over an adjacent polynya are very different [e.g., *Heinemann*, 1988]. The advection of cold continental air over relatively warm water leads to the development of a convective-thermal internal boundary layer (CIBL), which encompasses a rapid growth of the boundary layer height, a warming of the boundary layer, and a reduction of the surface sensible heat flux with fetch [e.g., *Chang and Braham*, 1991; *Brümmer*, 1997; *Renfrew and Moore*, 1999]. Observations show the reduction in surface turbulent

heat fluxes is systematic and significant, of order 20% over tens of kilometers and up to 50% over hundreds of kilometers. For simplicity, previous studies have either neglected these polynya-induced boundary layer modifications or made an unphysical uniform adjustment of the surface turbulent heat fluxes [e.g., *Cavaliere and Martin*, 1994; *Martin et al.*, 1998; *Markus et al.*, 1998; *Van Woert*, 1999; *Winsor and Björk*, 2000]. Here we improve on that approach by employing a CIBL model, devised by *Renfrew and King* [2000], to estimate the surface turbulent heat fluxes across the coastal polynya.

[7] The state variables extracted from the NWP analyses, or from the AWS, are also used to estimate the surface radiative fluxes via empirical formulae. Such formulae are frequently used in the polar regions and appear to work rather well, with the only significant uncertainty due to cloud cover [e.g., *Makhtas et al.*, 1999; *Van Woert*, 1999]. Unfortunately, satellite-retrieved cloud data, and for that matter satellite-based climatologies, are rather inaccurate in the polar regions. Hence previous studies have used these with reservations [e.g., *Markus et al.*, 1998; *Van Woert*, 1999; *Winsor and Björk*, 2000]. A more sophisticated approach is taken here as we employ an innovative statistical model, recently developed by *Makhtas et al.* [1999], which predicts cloud amount from temperature given climatological information about their distributions.

[8] In compiling this climatology every effort has been made to use observational data where possible or to model in a simple way known meteorological effects. However, a note of caution must be made given the paucity of in situ data from sites within polynyas. The surface energy budget estimates are as good as appears possible with the current generation of observing systems, but the uncertainties are still significant. The paper proceeds as follows: in section 2 the data sets used in the surface energy budget climatology are discussed in detail and the computational method is described. In section 3 a case study is presented illustrating a typical coastal polynya opening/closing episode off the Ronne Ice Shelf and how it is represented in our data sets. In section 4 a validation of the surface energy budget components for 1998 is presented. In section 5 the 7 year times series are presented, and ice production amounts are derived from the surface energy budget. Finally, in section 6 conclusions are presented.

2. Data Sets and Methodology

2.1. Polynya Area Data

[9] The polynya areas are derived from passive microwave satellite data from the Special Sensor Microwave Imager (SSM/I) using an iterative method as described in detail by *Markus and Burns* [1995]. They refer to this technique as the Polynya Signature Simulation Method (PSSM). The PSSM uses 85 and 37 GHz data (both horizontal and vertical polarizations) successively in order to take full advantage of the higher resolution at 85 GHz while compensating for its sensitivity to atmospheric effects with the lower resolution 37 GHz data. The pixel sizes are about 15 and 30 km for the 85 and 37 GHz channels, respectively. The method involves the classification of pixels into open water or sea ice using the 85 GHz channels and then a simulation of this pattern for the 37 GHz

channels, followed by a comparison with the measured 37 GHz channels. An iteration of these three steps is carried out until maximum agreement is reached. The 85 GHz data have been interpolated onto a 6.25×6.25 km grid. This does not provide additional information but does allow finer changes in open water area for each iteration step.

[10] Simulations of cloud coverage have shown that optically thick clouds can lead to an underestimation of PSSM-derived polynya areas of around 10%, which is the order of magnitude of which clouds influence the open water brightness temperature at 37 GHz (with respect to sea ice). This means that the sensitivity to weather effects in the algorithm is determined by the 37 GHz channels. The maximum ice thickness, which is included in the identified polynya area, is about 0.06 m. Land contamination effects are accounted for as the adjacent land is included in the simulation process explicitly via a prescribed land mask. For this study we have extended the PSSM technique to also estimate areas of thin or frazil ice. After calculating the open water area, as described above, we divide the sea ice pixels further into consolidated thick ice and thin or frazil ice by applying a new brightness temperature threshold. Note that smooth, thin ice and individual loose ice flows cannot be differentiated.

2.2. Meteorological Data

[11] In situ observational data for the atmospheric boundary layer over polynyas are rare because of the difficulty of placing and maintaining instruments in such locations. One has all the problems of working in the open ocean (e.g., a moving platform and the expense of aircraft or ship time), with the added discouragement that reaching the experimental area may be difficult or impossible because of the sea ice. Furthermore, global NWP models typically have a resolution of 100–200 km, so coastal polynyas are subgrid-scale to these models and therefore not represented in global analyses. Hence, instead of using meteorological data from over polynyas, we turn to meteorological data from onshore over the ice shelf, generally upwind of the coastal polynya. A number of AWS have been installed on the Ronne Ice Shelf at various times, although these do not encompass the full period of the climatology. Hence our approach has been to use NWP model analyses data, extracted from over the model ice shelf, and compare that with AWS data. The model data and energy budget results are checked against AWS data and energy budget results for selected periods. The atmospheric boundary layer over the coastal polynya can then be modeled using the ice shelf data as input to a boundary layer model.

[12] Data from two AWS on the Ronne Ice Shelf have been used (Figure 1). The British Antarctic Survey (BAS) Ronne Ice Shelf AWS was installed on 31 January 1998 at 75.5015°S , 58.069°W and records pressure, wind speed, and direction at 3 m and temperature and relative humidity at ~ 0.5 and ~ 2.5 m. A University of Wisconsin-built AWS named the Limbert-AWS was installed on 1 December 1995 at $\sim 75.42^\circ\text{S}$, 59.95°W and records pressure, wind speed, and direction at 3 m and temperature and humidity at ~ 2 m [e.g., *Stearns et al.*, 1993]. Unfortunately, for long periods the Limbert-AWS wind direction is constant, indicating a frozen anemometer and therefore unreliable wind data. In addition, the Limbert-AWS calibration has not been

checked since installation by BAS, and it appears the pressure sensor has drifted over time, and the relative humidity is unreliable.

[13] The choice of which NWP model to use was made difficult as at present all the models used by the major forecasting centers have some serious deficiencies in the polar regions [e.g., *Turner et al.*, 1999; *Bromwich et al.*, 1999; *Hines et al.*, 1999, 2000]. Data from both the European Centre for Medium-Range Weather Forecasts (ECMWF) operational analyses and the National Centers for Environmental Prediction (NCEP)/National Center for Atmospheric Research (NCAR) reanalyses were considered. On the face of it one might expect the higher-resolution ECMWF model to perform better; indeed, there is evidence from other studies that it can be more representative of high-latitude boundary layers [e.g., *Renfrew et al.*, 2002]. However, upon examination it was found that there was a large bias in the 2 m temperatures over the Ronne Ice Shelf. For example, comparing a year of AWS and ECMWF temperatures (1997/1998), the means were -22.3° and -12.1°C , respectively, and the linear regression slope was 0.56, indicating the model was too warm at low temperatures. The ECMWF model treated the ice shelves around Antarctica as permanent 1 m thick sea ice, rather than the reality of ice shelves of several hundred meters thickness. This designation as sea ice allowed a considerable conduction of heat through the sea ice from the relatively warm ocean below. For example, for an ocean-atmosphere temperature difference of 20°C , the heat conduction would be 50 W m^{-2} through 1 m thick sea ice compared to 0.5 W m^{-2} through 100 m of ice. A change to the ECMWF model was implemented on 1 April 1998 to correct this problem, but for the purposes of this climatology the ECMWF data set was not usable.

[14] The NCEP/NCAR reanalyses data are part of their project to reanalyze historic observational data (from upper air soundings, ground stations, satellite, aircraft, and so on) using a frozen data assimilation scheme and NWP model [e.g., *Kalnay et al.*, 1996]. The concept of a reanalyzed and therefore model-consistent data set is, of course, extremely attractive for climatological studies. The NCEP/NCAR reanalyses are at present the only reanalyses to cover the period of this study and in the end was the NWP data set that was chosen; however, that choice was not without reservations. Several studies have found a number of problems with the NCEP/NCAR reanalyses at high latitudes. For example, problems with a weak surface temperature inversion were found by *Bromwich et al.* [1999], radiative flux discrepancies caused in part by cloud misrepresentation are discussed by *Hines et al.* [1999], and problems in multi-decadal pressure time series are discussed by *Hines et al.* [2000]. *Renfrew et al.* [2002] found discrepancies in surface layer relative humidity and some problems representing low and high wind speeds over the ocean. We have noted problems in the interior of the large ice shelves with the development of patches of unrealistically low surface temperatures during calm, strongly stable conditions, perhaps indicative of too small a downward turbulent heat transport through the boundary layer. However, the NCEP/NCAR reanalyses did have a better representation of the large ice shelves than the ECMWF model had at that time. It was intended that the ice shelves were treated as "land" by the

model; however, this idea was not implemented, and instead, they were also set to permanent sea ice but of 3 m thickness rather than 1 m (R. Grumbine, personal communication, 1999). The 3 m ice thickness reduces the ice conduction to around one third of the 1 m conduction flux, which in turn reduces the biases in 2 m temperatures. *Hines et al.* [1999] noted an imbalance in the surface energy flux of roughly 20 W m^{-2} over the permanent ice shelves.

[15] As both models represented the large ice shelves as permanent sea ice, there was not a sharp transition in model surface temperatures across the ice shelf front, as one might expect. In the following comparison the nearest grid point to the BAS-AWS was used (-75.0°S , 58.025°W); this is almost exactly on the ice shelf front (Figure 1). Grid points north and south of this were also examined and found to be biased too warm and too calm, respectively. The coastal grid point used was taken as representative of the whole coastline; in other words the atmospheric boundary layer was assumed uniform along the coast. Although this is a crude approximation, it was felt the NWP model was not capable of resolving temperature structures across the ice shelf and that no biases would be introduced by this assumption.

[16] Figure 2 plots data from the two AWS and from the reanalyses for June and July 1998: (a) 2 m temperature (T_a) (b) mean sea level (msl) pressure, (c) wind speed, and (d) wind direction. The model wind speed is reduced from 10 to 3 m using standard surface layer similarity theory [e.g., *Smith*, 1988]. In general, the comparison is good; the phasing and magnitude of the AWS time series are usually captured by the model, although there are some discrepancies. To compare the full data sets, Figure 3 shows scatterplots of BAS-AWS data versus the nearest NCEP grid point. Overlain on each panel is a linear regression, taking the observed data as independent and the model data as dependent. Table 1 notes basic statistics for the time series, as well as the correlation coefficient r , the slope of the linear regression line, and the total rms error. The 2 m temperature is reasonably well modeled, $r = 0.81$, and the regression slope is 0.90, but there is a moderate amount of scatter in the comparison: the total rms error is 17.55°C . The low slope in the regression (i.e., the model not fully capturing cold periods) may be due to the conduction heat flux through the model ice shelf, as discussed above. There is a cluster of data around the 0°C mark: warmer temperatures than this at the surface will cause the ice shelf to melt and draw heat out of the boundary layer thus providing an in situ upper bound in temperature. Figure 3b shows msl pressure, which is very well modeled, with $r = 0.94$ and a regression slope of 0.92. There is a large amount of scatter in the wind speed, $r = 0.43$, and the linear regression does not fit the data well: there are many points where the model overestimates low wind speeds and underestimates high wind speeds. Figure 3d shows a heavy clustering in wind direction around 220° , i.e., directly offshore. This is believed to be primarily through a barrier-forced enhancement of the synoptic-scale flow [e.g., *O'Connor et al.*, 1994], which effects the surface flow in the western half of the ice shelf. Note there is a tendency for the model to force barrier wind directions when these are not observed, and this may explain the tendency for higher model winds than observed when wind speeds are low. Scatterplots for the Lambert-AWS versus NCEP reanalyses data are not

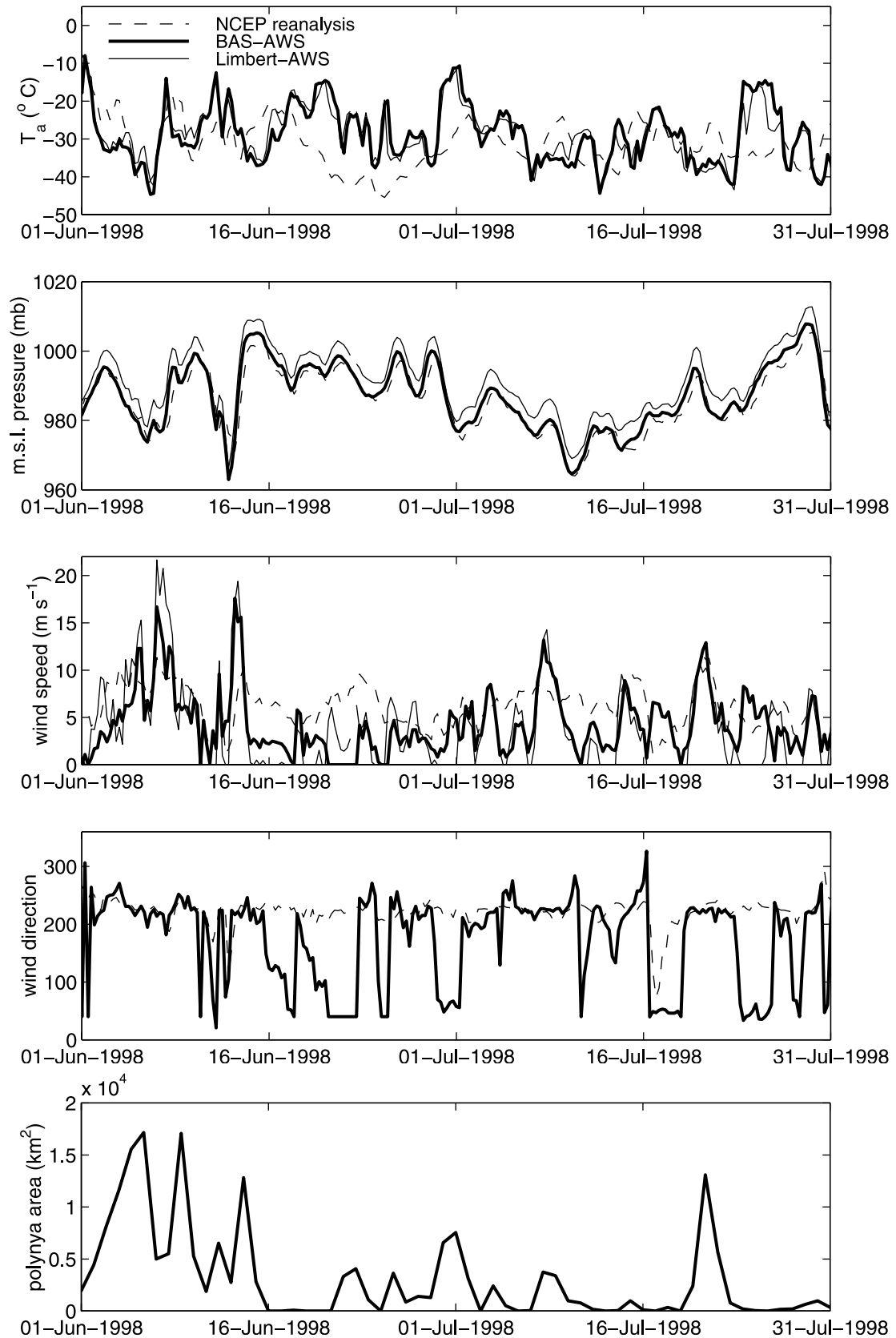


Figure 2. Time series of June–July 1998 showing data from the BAS-AWS and the Limbert-AWS and extracted from the NCEP/NCAR reanalysis: (a) 2 m air temperature, (b) mean sea level pressure, (c) 3 m wind speed, (d) wind direction, and (e) coastal polynya area from the PSSM data.

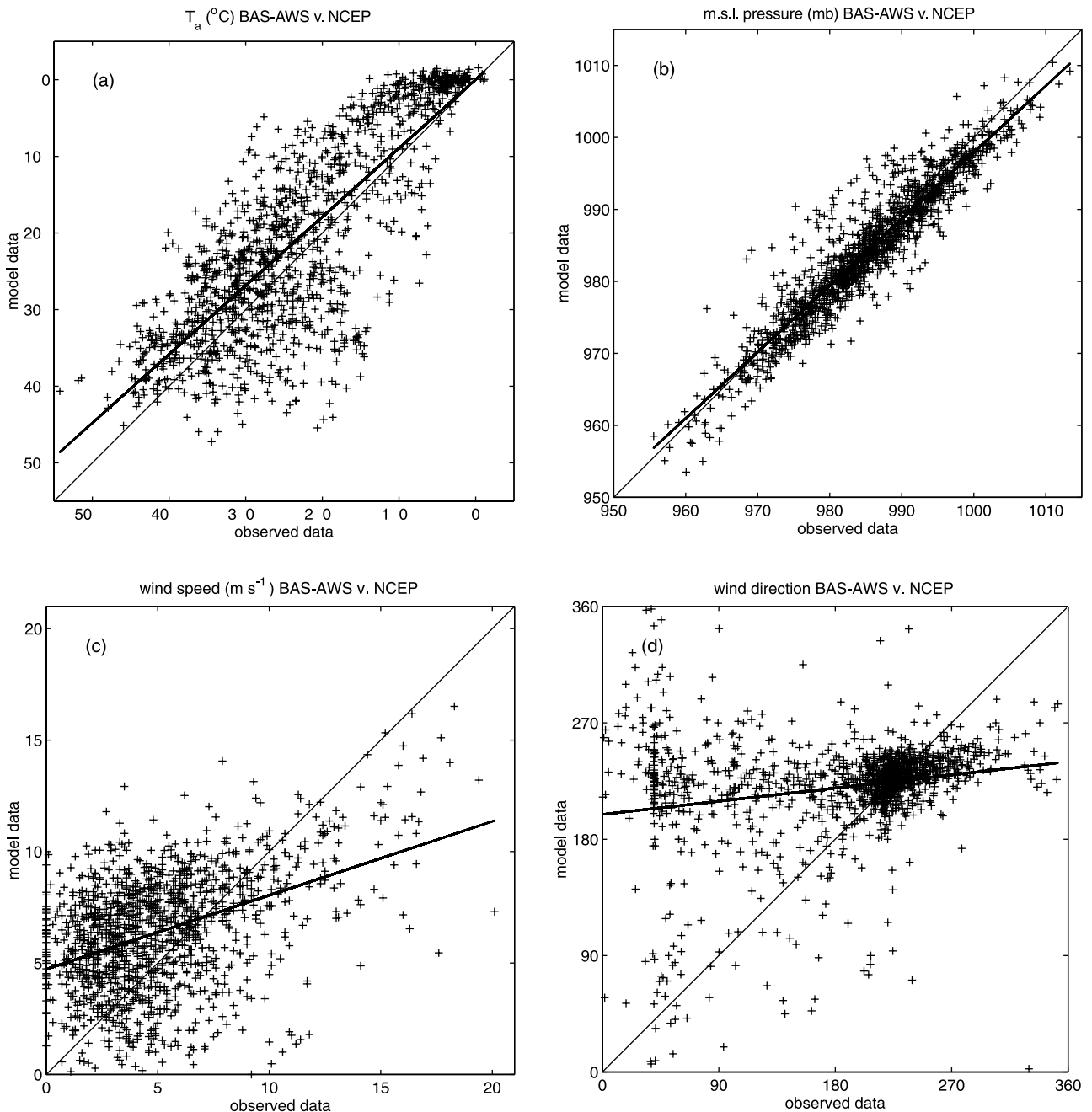


Figure 3. Scatterplots comparing data from the BAS-AWS and from the NCEP/NCAR reanalysis: (a) 2 m air temperature, (b) mean sea level pressure, (c) 3 m wind speed, and (d) wind direction. The period of comparison is 1 February to 31 December 1998. A linear regression line is overlain.

shown, but some statistics are tabulated in Table 2. The T_a plot is qualitatively similar to Figure 3a, with the model mean around 3°C too warm and again a moderate amount of scatter. The msl pressure plot has little scatter but a bias error of 5 mbar, as mentioned earlier. This is thought to be due to a drift in the Limbert-AWS calibration over the 2–3 years since installation. A comparison between the two AWS for their overlap period (not shown) indicates an excellent correspondence in T_a , a correlation of 0.95, a regression slope of 0.90, and a bias of only 0.1°C . Thus we can assume the AWS are representing the boundary layer

temperature of the area well. There is a reasonable correspondence in wind speed, $r = 0.65$ and a regression slope of 0.83, but a fair amount of scatter, perhaps illustrating the difficulty of representativeness in point wind measurements either between two adjacent sites or between point measurements and models.

[17] In general, the quality of the model ice shelf temperature, pressure, and wind data is acceptable given the paucity of data entering the NWP assimilation system, the relatively coarse model grid, and the inevitable problems in model physics. For use in comparing components of the

Table 1. A Comparison of Meteorological Data From the Ronne Ice Shelf BAS-AWS and Extracted From the NCEP/NCAR Reanalysis Data Set for the Period 1 February to 31 December 1998

	T_a , °C	Msl Pressure, mbar	Wind Speed, m s^{-1}	Wind Direction	Data Set
Mean	-23.29	985.3	5.08	184.7	BAS-AWS
	-20.85	984.3	6.41	220.1	NCEP
Standard deviation	11.62	9.6	3.38	76.0	BAS-AWS
	12.93	9.4	2.62	40.4	NCEP
Maximum	1.16	1013.4	20.10	...	BAS-AWS
	1.55	1010.4	16.52	...	NCEP
Minimum	-54.24	955.6	0	...	BAS-AWS
	-47.25	953.5	0	...	NCEP
Correlation coefficient	0.81	0.94	0.43	0.21	BAS-AWS versus NCEP
Regression slope	0.90	0.92	0.33	0.11	BAS-AWS versus NCEP
Total rms error	17.55	13.5	4.47	93.0	BAS-AWS versus NCEP

surface energy budget (i.e. Q_s , Q_b , and Q_r) a 1 year AWS time series for 1998 was generated by splicing the January data from the Limbert-AWS (manually checked for bad wind readings) with the February to December data from the more reliable BAS-AWS. This AWS time series is used later to provide a benchmark for the 7 year model or NCEP time series.

2.3. Turbulent Heat Fluxes

[18] To calculate the surface turbulent heat fluxes within a polynya, we require surface layer meteorological variables (i.e., T_a , pressure, relative humidity, and winds) to use as input to standard bulk formulae. The easiest approach would be to use the AWS or NCEP ice shelf time series and assume it represented the atmosphere over the polynya. However, it is clear that as cold air flows over the relatively warm polynya waters, the air will warm, and the surface heat exchange will be systematically modified. The atmosphere develops a CIBL because of the change in surface heating [e.g., Garratt, 1992]. Observations of such cold air outbreaks show an increase in CIBL height h , a substantial warming of the boundary layer, and a consequent reduction in the surface sensible heat fluxes with fetch [e.g., Grossman and Betts, 1990; Chang and Braham, 1991; Brümmner, 1997; Renfrew and Moore, 1999]. These modifications are primarily due to heat flux convergence with secondary effects due to radiative flux convergence and microphysical processes (e.g., the formation of fog, clouds, precipitation, and so on).

[19] In a previous paper we have described a CIBL model of this boundary layer modification [Renfrew and King, 2000]. Here we use this model to calculate the surface turbulent heat fluxes (Q_s and Q_t in (1)) as a function of distance across the polynya. The model follows the simple one-dimensional mixed layer slab model discussed, for example, by Garratt [1992]. A sketch is presented in Figure 4. The conservation of potential temperature equation is solved by equating advection by the mixed layer wind u_m with turbulent heat flux convergence and assuming steady state conditions. An equation for the jump in mixed layer potential temperature θ_m at the CIBL top is also required. The model extends those of, for example, Venka-

tram [1977], Gamo et al. [1983], and Stunder and Sethuraman [1995] by allowing both θ_m and Q_s to vary with fetch. The boundary layer warming then alters the flux convergence and hence affects further the boundary layer growth. For simplicity, secondary effects such as radiative flux convergence and microphysical processes are neglected in the model. Following Figure 4, let us take (x, y, z) as a coordinate system with x oriented offshore (i.e., fetch), y oriented along the coast, and z oriented in the vertical. Equations for $\theta_m(x)$ and $h(x)$ are solved by numerical integration and an iteration scheme, with a bulk formulation required to calculate $Q_s(x)$ and close the solution set. Surface layer temperature, pressure, and winds are input variables to the model, with the initial boundary layer height h_0 , an entrainment coefficient β , and an initial stability profile γ_{sl} and γ_θ set as parameters. Renfrew and King [2000] discuss the model's sensitivity to these parameters and show that although the CIBL height h can be highly sensitive to the choice of stability profile, the surface fluxes are considerably less sensitive to the choice of this parameter.

Table 2. A Comparison of Meteorological Data From the Limbert-AWS and Extracted From the NCEP/NCAR Reanalysis Data Set for the 2 Year Period 1 January 1997 to 31 December 1998^a

	T_a , °C	Msl Pressure, mbar	Data Set
Mean	-23.92	992.6	Limbert-AWS
	-20.89	987.9	NCEP
Standard deviation	11.74	10.0	Limbert-AWS
	13.22	10.0	NCEP
Maximum	5.80	1018.9	Limbert-AWS
	1.55	1012.4	NCEP
Minimum	-52.33	960.9	Limbert-AWS
	-52.15	956.9	NCEP
Correlation coefficient	0.86	0.93	Limbert-AWS versus NCEP
Regression slope	0.97	0.90	Limbert-AWS versus NCEP
Total rms error	17.93	14.64	Limbert-AWS versus NCEP

^aNote the wind speed and direction statistics are not tabulated as the vane was frozen for long periods.

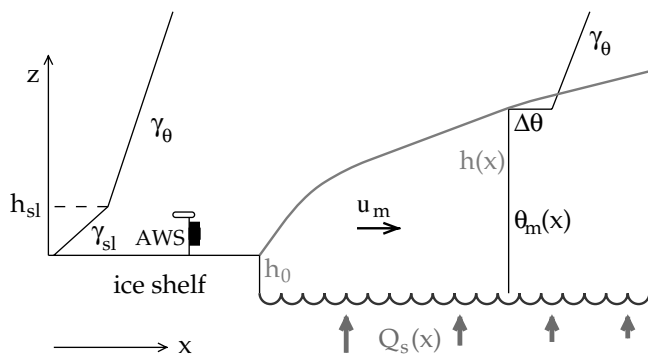


Figure 4. A sketch of a CIBL development for a cold air outbreak over a polynya. The *Renfrew and King* [2000] model predicts CIBL height $h(x)$, mixed layer potential temperature θ_m , and surface sensible heat flux $Q_s(x)$ from upstream surface data given an initial CIBL height h_0 , a surface layer height h_{sl} , and stabilities γ_θ and γ_{sl} .

Validations showed $Q_s(x)$ is well modeled for clear-sky conditions; where the neglected secondary effects are more important, or over longer fetches, the model appears to capture around 75% of the boundary layer warming.

[20] The surface sensible and latent heat fluxes are calculated using standard bulk flux algorithms [e.g., *Smith*, 1988; *Garratt*, 1992]:

$$Q_s(x) = C_H \rho(x) c_p U_{10} [\theta_{SST} - \theta_m(x)] \quad (2)$$

$$Q_l(x) = C_E \rho(x) L U_{10} [q_{sat} - q_a(x)], \quad (3)$$

where ρ is the air density, c_p is the specific heat at constant pressure for air, U_{10} is the 10 m wind speed, θ_{SST} and θ_m are the potential temperatures of the polynya sea surface temperature and the mixed layer atmosphere, L is the latent heat of vaporization, q_{sat} is the saturated specific humidity at the sea surface temperature, q_a is the specific humidity at the mixed layer air temperature, and C_H and C_E are exchange coefficients. A positive flux means a warming of the atmosphere and a cooling of the ocean. The exchange coefficients are taken from *DeCosmo et al.* [1996], and the bulk algorithm is based upon *Smith* [1988], which is suitable for heat exchange over open water polynyas beyond any microscale effects at the polynya edge [*Andreas and Murphy*, 1986; *Smith et al.*, 1990]. This particular bulk algorithm is well established and has been recently verified for a high-latitude cold air outbreak data set [*Renfrew et al.*, 2002]. The CIBL model provides $\rho(x)$, $\theta_m(x)$, and U_{10} from the AWS or NCEP input data. The specific humidity $q_a(x)$ is calculated assuming that the surface layer is saturated with respect to ice, i.e., the relative humidity with respect to ice RH_i is 100%. This is an excellent assumption for ice shelves during the cold winter months, as noted recently by *King and Anderson* [1999]. They found the monthly mean RH_i varied between 95 and 100% during the winter period, falling to around 90% in the summer. Examining the humidity data for the BAS-AWS (not shown), the mean RH_i was 97.9%, and for the vast majority of the time the $RH_i = 100\%$, providing

further evidence that this is a good assumption. Recall that specific humidity is strongly dependent on temperature, so changes to RH when the temperature is very low are somewhat unimportant.

[21] In calculating the surface energy budget climatology, several CIBL model parameters have to be specified. In particular, the entrainment parameter β was set to 0.2, and the initial CIBL height was set to $h_0 = 40$ m, the approximate height of the ice shelf. The sea surface temperature was set to -1.8° , -1.7° , -1.5° and -1.7°C in winter, spring, summer, and autumn, respectively (K. Nicholls, personal communication, 2000). *Renfrew and King* [2000] assumed a linear temperature profile, and so, the ambient stability was simply set as a constant. For the climatology we have adopted a piecewise linear temperature profile (Figure 4), defined by a strongly stable surface layer (stability γ_{sl}) of height h_{sl} and a stable free atmosphere (stability γ_θ). The γ stability parameters were set using seasonal and wind speed-based criteria (Table 3) following climatological guidance obtained from meteorological tower data [*King*, 1990] and from radiosonde sounding data [*King et al.*, 1998]. The use of piecewise linear temperature profiles means there are rapid changes in CIBL growth rate when $h(x)$ reaches h_{sl} , but as noted above, the consequent changes in $Q_s(x)$ are relatively small.

2.4. Radiative Heat Fluxes

[22] The surface net radiative flux Q_r in (1) is found by adding the four components:

$$Q_r = \text{LWU} - \text{LWD} + \text{SWU} - \text{SWD}, \quad (4)$$

where LWU and LWD are the upwelling and downwelling longwave components and SWU and SWD are the upwelling and downwelling shortwave components. Hence a positive flux indicates a cooling of the surface. We calculate the longwave and shortwave components using empirical formulae. Such formulae are functions of near-surface temperature and cloud fraction (N) as well as latitude and time for SWD. Previous studies have shown them to be surprisingly accurate [e.g., *Makshtas et al.*, 1999], and they have been heavily used in the polar regions where observational data are scarce and model parameterizations are less well tested. The greatest problem with these formulae is in determining a cloud fraction when observations are

Table 3. The CIBL Model Parameters γ_θ and γ_{sl} As Prescribed by Seasonal and Wind Speed Criteria^a

Season	Wind Speed, m s^{-1}	h_{sl} , m	γ_θ , K km^{-1}	γ_{sl} , K km^{-1}	Temperature Inversion, K
Winter	0–5	50	9.2	200	10.0
	5+	100	9.2	25	2.5
Spring	0–5	100	9.2	50	5.0
	5+	100	9.2	10	1.0
Summer	0–5	100	6.7	10	1.0
	5+	100	6.7	6.7	0.67
Autumn	0–5	50	9.2	150	7.5
	5+	100	9.2	25	2.5

^aThe parameter values are suggested by climatological studies of the nearest manned meteorological station at Halley, on the Brunt Ice Shelf. The height of the strongly-stable surface layer (h_{sl}) and its prescribed stability γ_{sl} define the magnitude of the temperature inversion.

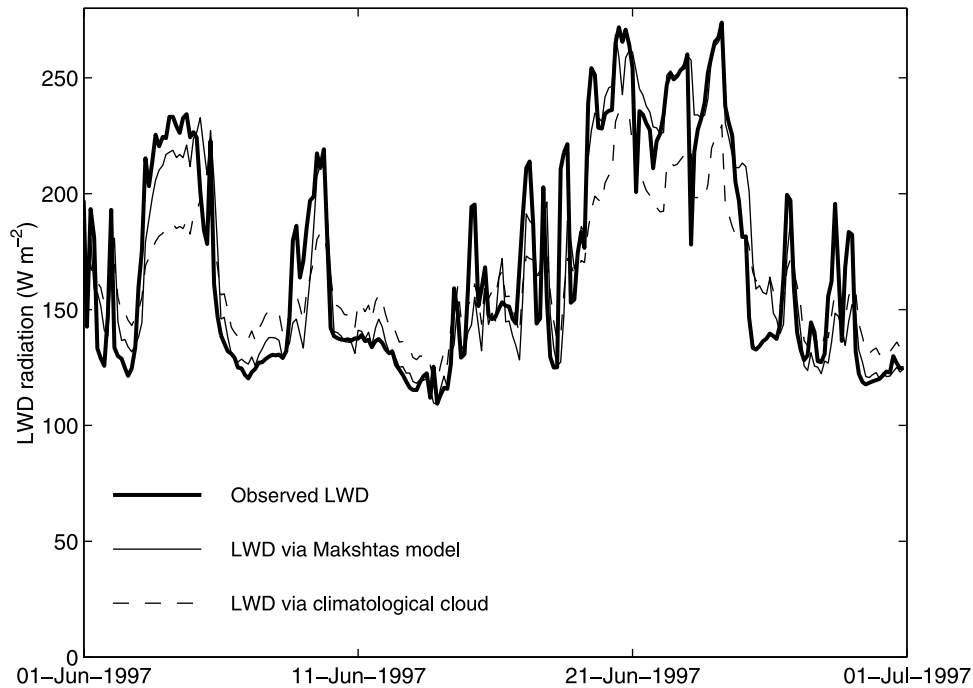


Figure 5. Time series from June 1997 of LWD radiation at Halley Base. The plot compares the observed LWD with those calculated via (5) using the *Makshtas et al.* [1999] cloud model and using a climatological cloud cover.

unavailable. In addition, for the polar regions, using satellite-based cloud covers poses problems because of the similarity in brightness temperatures between snow/ice surfaces and clouds, as well as the irregular coverage of polar-orbiting satellites. Previous surface energy budget studies have been forced to set constant, or monthly mean, cloud fractions using climatological data [e.g., *Martin et al.*, 1998; *Markus et al.*, 1998; *Van Woert*, 1999; *Winsor and Björk*, 2000]. Here we are able to improve on that approach by incorporating an innovative statistical model, following *Makshtas et al.* [1999], which determines cloud amount using only surface temperature. The model is based upon the close coupling between cloud cover and temperature in the polar winter. In the polar regions, cloud amount has a U-shaped distribution, whereas temperature has a normal distribution. *Makshtas et al.* developed an algorithm to predict the cloud amount from the temperature and still produce a U-shaped distribution. A beta distribution is fitted to the cloud distribution, for which two shape parameters are required. To determine shape parameters for our area of interest we use the 42 years of climatological data (1957–1999) available from the nearest manned base at Halley, on the Brunt Ice Shelf (Figure 1). It is assumed that this will be representative of the edge of the Ronne Ice Shelf. Following *Makshtas et al.* [1999], the shape parameters were computed monthly. One shortcoming of the model is that it is really only applicable when cloud cover and surface temperature are closely coupled, i.e., during the polar winter months. It is less applicable when shortwave radiation is a major term in the surface energy budget. This shortcoming is reflected by the fact that the algorithm derived by *Makshtas et al.* is only valid when both shape parameters are <0.5 . For the Halley cloud data

this was the case from April to September but not for October to March. After some consideration we decided to use the *Makshtas et al.* cloud model for October to March but with the winter mean shape parameters.

[23] The benefit of using the *Makshtas et al.* [1999] model is illustrated in Figure 5, which shows three LWD time series for June 1997 at Halley. The observed data, the LWD calculated via the cloud model, and the LWD calculated using a climatological cloud amount are shown. It is clear that the cloud model greatly improves the LWD estimates; indeed, the match is excellent: the largest error is only around 10 W m^{-2} for changes of 10 times that amount. Using the climatological cloud amount, one underestimates during high LWD periods (cloudy skies) and overestimates during low LWD periods (clear skies).

[24] The *Makshtas et al.* [1999] cloud model is used to create time series of cloud amount for the Ronne Ice Shelf area using T_a from the AWS and NCEP time series. The modeled cloud amount distributions were examined by season (not shown): the winter histogram was U-shaped as observational studies of the Weddell Sea region would corroborate [e.g., *Makshtas et al.*, 1999]. The spring, summer, and autumn histograms, however, were all biased toward full cloud cover, an effect of pushing the cloud model into an area of questionable use. With regard to this it is worth noting two mitigating points. First, such a bias is somewhat self-compensating in the summertime as a cloud-filled atmosphere will increase LWD but reduce SWD. Second, for cold air outbreaks over coastal polynyas one would expect enhanced cloud amounts because of the development of shallow convective cloud within the boundary layer; hence a bias to the cloudy side may not be too unrealistic for coastal polynyas.

[25] The radiative heat flux components are calculated as follows. The LWD is calculated following *König-Langlo and Augstein* [1994]:

$$\text{LWD} = \sigma T_a^4 (0.765 + 0.22N^3), \quad (5)$$

where σ is the Stefan-Boltzmann constant ($5.67 \times 10^{-8} \text{ W m}^{-2} \text{ K}^{-4}$), T_a is the 2 m temperature, and N is the cloud amount as calculated above. This formula performed the best of those tested by *Makshatas et al.* [1999]. Over a coastal polynya, where T_a will be modified by air-sea fluxes as described earlier, it is not clear whether one should use the upwind or the modified T_a in (5). To answer this, the Streamer radiative transfer model [*Key and Schweiger*, 1998] was used to compute LWD for a typical Halley winter radiosonde profile under clear skies. A good correspondence was found between the observed LWD, the radiation model results, and those from (5): the LWD was 134, 138, and 142 W m^{-2} , respectively. To simulate the modification of this profile by a coastal polynya, the lowest 200 m of the profile was mixed to neutral and then 0, 5, 10, and 15 K were added to the mixed layer temperature to simulate the CIBL warming. The LWD was then recalculated for these four modified profiles with the radiation model and using (5) with the modified T_a . The results show that using (5) with the modified T_a overestimates the LWD by up to 50 W m^{-2} . On the other hand, simply using (5) with the upwind T_a and assuming a constant LWD flux across the polynya only produces errors of $0\text{--}23 \text{ W m}^{-2}$. As most temperature changes will be of the order 5 K for typical polynya widths [*Renfrew and King*, 2000], these results suggest using a constant LWD calculated from the upwind T_a is an excellent approximation, i.e., accurate to within 5 W m^{-2} .

[26] The LWU is calculated as

$$\text{LWU} = \varepsilon \sigma T_{\text{SST}}^4, \quad (6)$$

where ε is the surface emissivity ($\varepsilon = 0.97$) and T_{SST} is the seasonally prescribed sea surface temperature as above.

[27] The clear-sky SWD follows that described by *Zillman* [1972], as suggested by *Curry and Webster* [1999]:

$$\text{SWD}_{\text{CLEAR}} = \frac{S_0 \cos^2 Z}{1.085 \cos Z + (2.7 + \cos Z)e_a + 0.01}, \quad (7)$$

where S_0 is the solar constant set to 1370 W m^{-2} , Z is the solar zenith angle, and e_a is the vapor pressure in bars. The solar zenith angle is a function of latitude and time of year and is easily calculated using standard formulae [e.g., *Curry and Webster*, 1999]. The effect of clouds is included following *Reed* [1977], as suggested by *Curry and Webster* [1999]:

$$\text{SWD} = [1 + 0.0019(90 - Z) - 0.62N]\text{SWD}_{\text{CLEAR}}, \quad (8)$$

where N is the cloud amount.

[28] The SWU is simply

$$\text{SWU} = \alpha \text{SWD}, \quad (9)$$

where the albedo α is set constant at 0.08, a good assumption for the sea during overcast conditions [e.g., *Curry and*

Webster, 1999]. All four radiative flux components are constant over the coastal polynya domain and so are simply added to obtain a net radiative flux (equation (4)).

2.5. Computational Procedure

[29] The area covered by the climatology is the southern part of the Weddell Sea along the Ronne Ice Shelf. The computational domain is defined by the PSSM data set and consists of 60×100 grid squares ($6.25 \times 6.25 \text{ km}$). We define the offshore and alongshore directions as the x and y directions respectively. The domain is oriented such that the offshore direction is 50° clockwise from north, so approximately perpendicular to the Ronne Ice Shelf front (Figure 1).

[30] The surface energy budget for coastal polynyas within this domain is calculated from (1), rewritten here as

$$\begin{aligned} Q_{\text{tot}}(x, y, t) = \rho_i L_f F(x, y, t) = \text{PSSM}_{\text{MASK}}(x, y, t) \\ \times [Q_s(x, t) + Q_l(x, t) + Q_r(t)] \end{aligned} \quad (10)$$

where $\text{PSSM}_{\text{MASK}}$ is the surface category sea ice, land, thin ice, or open water, as described in section 2.1. If the categorization of a pixel is as land or as sea ice, then all the right-hand side fluxes are assumed zero. In other words, the climatology is only for coastal polynyas within the domain. Recall that observational and modeling studies have shown that the atmosphere-ocean energy transfer through consolidated sea ice is orders of magnitude smaller than through leads or polynyas [e.g., *Smith et al.*, 1990].

[31] For each day the PSSM data set is used to define pixels that are part of coastal polynyas, i.e., open water or thin ice and adjacent to the coastline. The AWS or NCEP time series is then assumed to represent the atmosphere at the upstream edge of this coastal polynya and is used as input to the CIBL model. If the wind is offshore, the CIBL model is run out to a fetch of 360 km, at 1 km resolution; the surface fluxes are then interpolated onto the 6.25 km grid. The offshore component of the mixed layer wind speed u_m is used to grow the CIBL. If the $\text{PSSM}_{\text{MASK}}$ is land or sea ice, then the fluxes are zero; if the mask is open water, the turbulent fluxes are as given by (2) and (3); and if the mask is thin ice, the turbulent fluxes are multiplied by a coefficient (set to 0.7) to imitate the effect of the thin ice surface. In other words, the turbulent heat fluxes through the layer of thin ice were assumed to be around 70% of those for open water. This value was chosen on the basis of the modeling study of *Alam and Curry* [1998]. If the wind is onshore, the CIBL model is not used, and instead, the surface fluxes are calculated for the ice shelf edge and assumed constant over the computational domain. Hence, in general, Q_s and Q_l vary with fetch and time, whereas the Q_r term varies only with time. As the $\text{PSSM}_{\text{MASK}}$ varies with x and y , the total surface energy budget and thus the ice production rate is a function of (x, y, t) . The final Q_{tot} or F data are 6 hourly, although note the PSSM data are daily. Time series using both the 1 year AWS input data and the 7 year NCEP input data were calculated.

3. An Illustrative Case Study

[32] We now examine a coastal polynya opening/closing episode for the southern Weddell Sea using the data sets

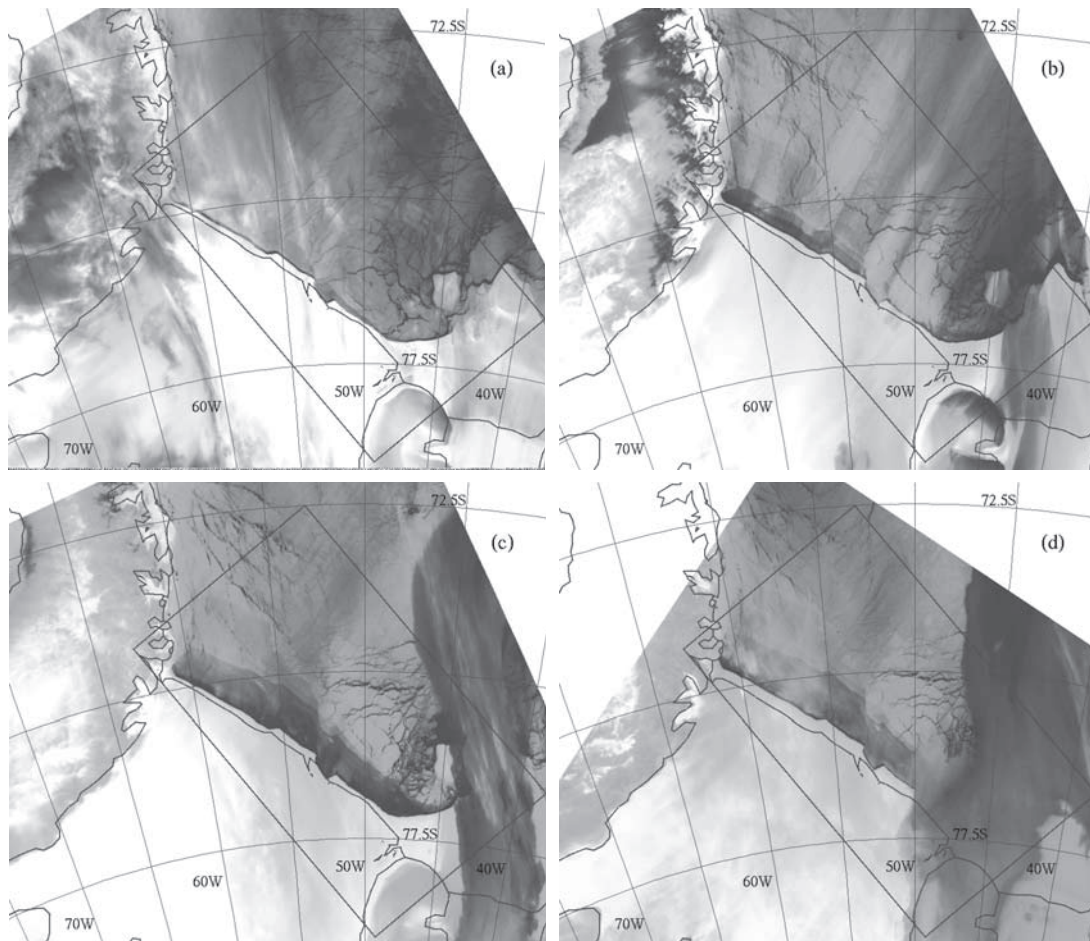


Figure 6. Infrared AVHRR satellite images of the southern Weddell Sea and the Ronne Ice Shelf, processed so that white is cold and black is warm: (a) 19.53 UTC 19 July 1998, (b) 19.42 20 July 1998, (c) 19.30 21 July 1998, and (d) 3.51 UTC 22 July 1998. The images show a coastal polynya opening episode, with sea ice being blown off the ice shelf, exposing a belt of warmer open water underneath. The inner rectangle superimposed on the image shows the area processed via the PSSM algorithm. Note the dark band on the right of Figures 6b–6d, is a due to a relatively warm band of cloud.

described in section 2. Figure 6 shows four infrared satellite images from the advanced very high resolution radiometer (AVHRR) system, flown onboard the NOAA polar orbiting satellites, and received at the BAS's Rothera station. The image resolution is 1.1 km. The images have been processed so that lighter colors are colder brightness temperatures and darker colors are warmer brightness temperatures. So, for example, the Ronne Ice Shelf is colder than the Antarctic Peninsula (to the west) because of a strong temperature inversion in the boundary layer over the ice shelf, while offshore the mid-temperature (shaded) sea ice is cracked with warmer (darker) leads. Figure 6 shows a sequence of four images from 19 to 22 July 1998. Examining the sequence, the opening of a belt of open water/thin ice along the ice shelf front is clear; developing from a narrow shore opening in Figure 6a on 19 July, through to its greatest extent in Figure 6c on the 21 July. Note that in Figure 6c the decrease in brightness temperature with distance offshore is indicative of an increase in frazil ice density, or ice thickness, across the polynya. By Figure 6d, early on 22 July, the polynya has stopped expanding in area and appears to be

colder (i.e., more frozen over), although this is difficult to ascertain as cloud is forming over the polynya and indeed later images are wholly masked by cloud (illustrating the limitations of infrared imagery for such studies). Focussing on Figure 6c, one might imagine the dark band on the right of the images is a katabatic surge event [e.g., *Bromwich et al.*, 1992], but an examination of large area images (not shown) and Figures 6a, 6b, and 6d show, the warm band over Berkner Island, over 500 m in height, and as clearly a cloud feature rather than a surface feature.

[33] The polynya opening episode is clear in Figure 7, which shows a sequence of four passive microwave images processed via the PSSM algorithm (section 2.1). Each image should be regarded as a daily average, as each is processed from several satellite passes. Figure 7 shows daily averages from the 19, 20, 21, and 22 July 1998. On the 19 July the PSSM-processed region is entirely sea ice. Over the 20 and 21 July a thin belt of open water/thin ice opens along the ice shelf front. Note the polynya appears somewhat offshore because of the land mask “drift;” that is, a land mask has to be supplied to the algorithm, and this becomes out of date as

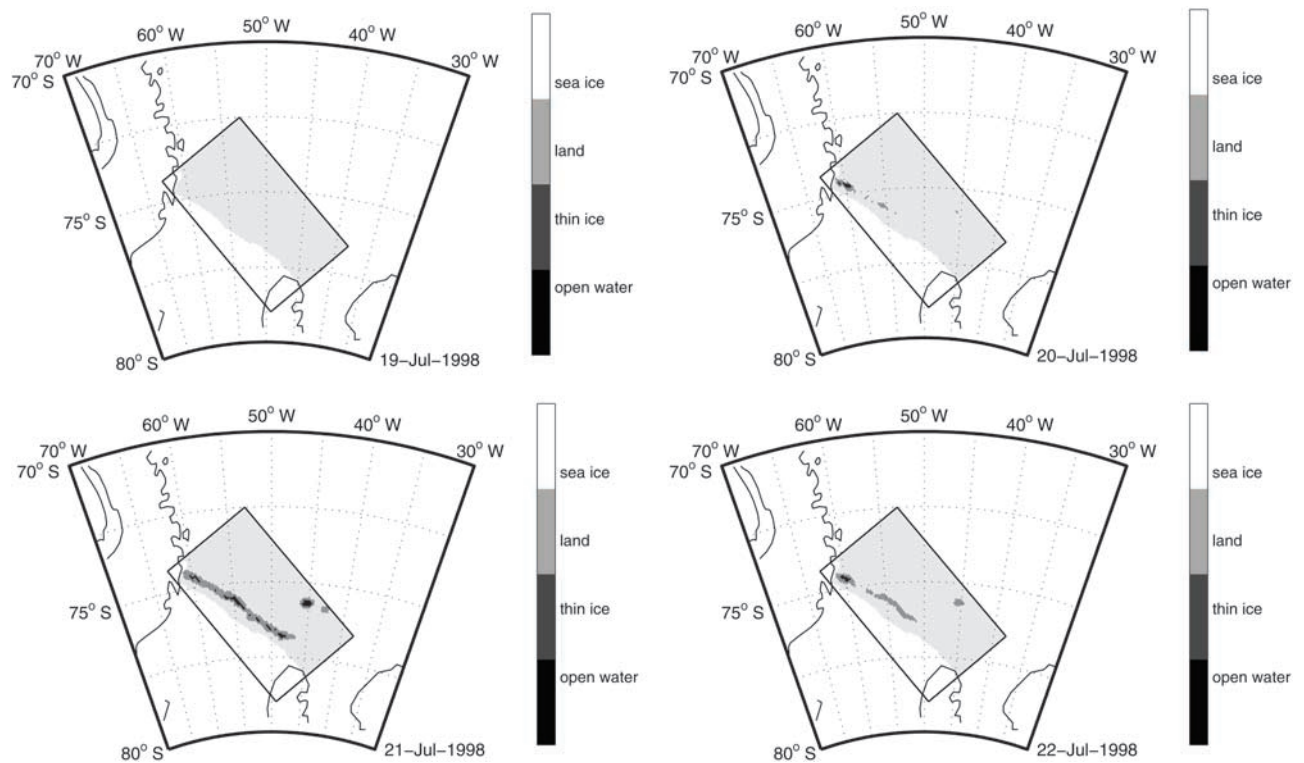


Figure 7. Maps of sea ice cover as determined by the PSSM algorithm from SSM/I passive microwave brightness temperatures: (a) 19, (b) 20, (c) 21, and (d) 22 July 1998. The inner rectangle shows the region processed. The algorithm differentiates regions of open water and thin ice from those of thicker sea ice.

the ice shelves advance or retreat. In this case a thin strip of ice shelf is shaded as sea ice in Figure 7; there is a similar mask drift in Figure 6. By 22 July the polynya is shrinking in area, and by the 23 July (not shown) the region is entirely sea ice again. Comparing Figure 6 and Figure 7, the correspondence is extremely good, both in terms of location and polynya area. A more detailed comparison between infrared, passive microwave, and active microwave (synthetic aperture radar) is carried out by *Markus and Burns* [1995].

[34] The polynya opening is coincident with the dramatic deepening of a low-pressure system located in the central Weddell Sea. Figure 8 shows msl pressure plots for 18 UTC on 19, 20, 21, and 22 July, approximately coincident with the infrared images of Figure 6. The data are from the NCEP/NCAR reanalyses project (section 2.2). Figure 8 shows the low-pressure system deepening from 960 to 942 mbar in 24 hours. The cyclonic circulation induced by the low-system forces offshore winds over the whole Ronne Ice Shelf. Geostrophically, these are strongest at 18 UTC 20 July (Figure 8b), just prior to the greatest polynya area on 21 July (Figures 6c and 7c). The same wind distribution is clear in vector plots of model 10 m winds (not shown). By 22 July the low has filled considerably, and the winds have dropped. The timing of the low-pressure system's rapid development and the ensuing strong offshore winds suggest that this event leads directly to the opening of the coastal polynya.

[35] The polynya event is clearly defined in the AWS and NCEP meteorological time series of Figure 2. Over 19–21 July there is a well-defined drop in pressure and a dramatic

increase in wind speed from around 0 to 13 m s^{-1} . The wind direction is offshore, at 220° , and the air temperatures are measured at about -37°C . The NCEP model does a reasonable job of capturing this event; the increase in wind speed is correct in both magnitude and timing, and the wind direction is accurate. The model temperatures are broadly correct until the winds drop, and then the model becomes too warm.

[36] Figure 2e plots a time series of coastal polynya area for the June–July 1998 period, calculated from the PSSM data. The coastal polynya area is calculated by summing pixels from the PSSM data, which are then checked for whether the open water/thin ice is near the coast (within 16 pixels) or adjacent to another open water/thin ice pixel (within four pixels). This eliminates offshore openings in the sea ice, which should not be part of our coastal polynya climatology. For example, the open water at 76°S , 45°W in Figure 7, also visible as open water in the lee of a major iceberg in Figure 6, is not included in the coastal polynya area time series. In Figure 2, the 19–22 July episode is clearly seen as a rapid opening and closing; the peak area is $13,000 \text{ km}^2$ ($\sim 450 \times 30 \text{ km}$, Figure 6c). Examination of this time series shows all of the large polynya areas are coincident with moderate to strong offshore wind events and generally a rapid change in pressure, for example, those in the first half of June. However, the relationship is not one to one: strong offshore winds can lead to only moderate polynya openings (e.g., 10–12 July), and moderate offshore winds can lead to large polynya openings (e.g., 1 July). Further discussion of the dynamics of coastal polynyas is

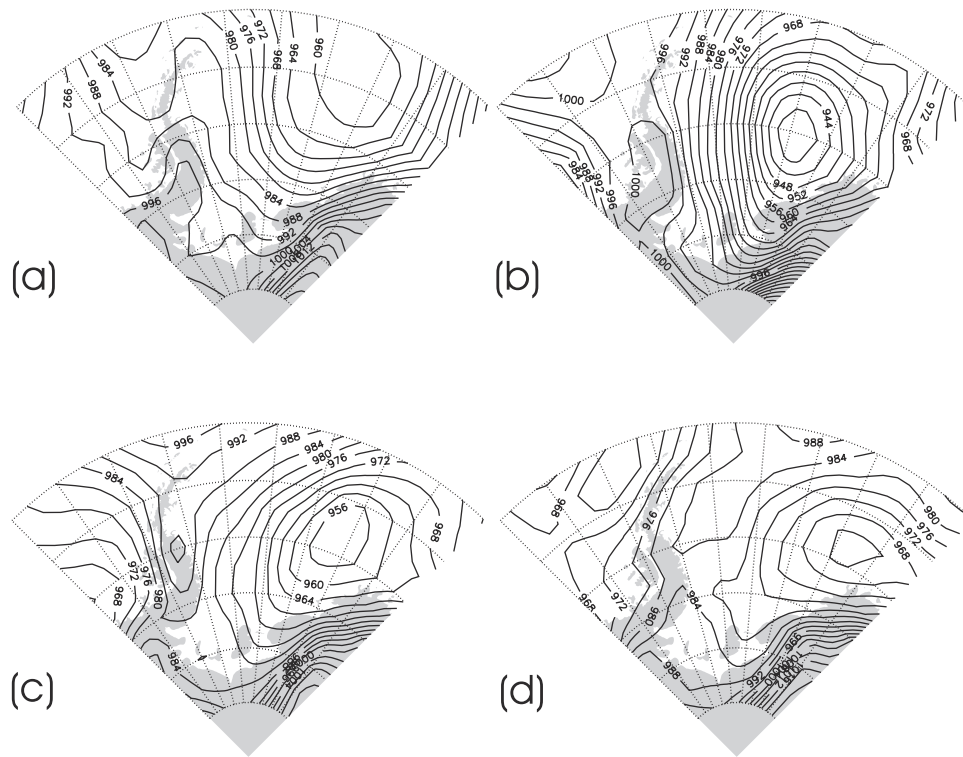


Figure 8. Maps of msl pressure for the Weddell Sea region from the NCEP/NCAR reanalyses (interval 4 mb) at 18 UTC on (a) 19, (b) 20, (c) 21, and (d) 22 July 1998.

reserved for future studies (or see Pease [1987], Markus and Burns [1995], Wilmott *et al.* [1997], and Van Woert [1999]). The July 1998 polynya opening event illustrated here shows a coherent picture through the different data sets and provides at least a qualitative assurance of being able to represent such events.

4. A Validation of the Surface Energy Budget Components

[37] The surface energy budget components for the AWS and the NCEP model time series are calculated as described in section 2. For comparison purposes, Figure 9 shows June and July 1998 (the same period shown in Figure 2) for the mean Q_s , Q_l , Q_r , and Q_{tot} components, where the mean is over the coastal polynya area. The Q component time series are characterized by periods of positive heat fluxes (oceanic cooling) interspersed with periods of zero fluxes when there is no coastal polynya present. Over these 2 months the sensible heat flux is the largest term and dominates the total heat flux. The Q_r component is also positive and is less variable than the turbulent fluxes. In general, the AWS and model time series correspond quite well, both in the amplitude and phasing of the Q components. There are periods when the correspondence is poor, and compared with Figure 2, these can be traced back to errors in the NCEP meteorological data. For example, the NCEP fluxes are much too high around 22–25 June and remain generally too high until early July. Compared with Figure 2, the NCEP model is too cold for most of this period, and around 22–25 June the model wind speed is perhaps 5 m s^{-1}

greater than the observed. Over the 2 month period, Q_r compares most favorably because of its dependence only on T_a , rather than on both T_a and wind speed.

[38] A comparison of the AWS and model time series for the whole of 1998 is summarized in Table 4; both year-long time series and scatterplots have also been examined but for brevity are not reproduced here. First, it is worth commenting on the large range in Q_{tot} : the time series minima are around -350 W m^{-2} during the summer period, when the SWD term dominates; the maxima are around $1100\text{--}1200 \text{ W m}^{-2}$ during the winter period, when the Q_s term is largest and all three Q terms are positive. This range is extremely high, certainly larger than in midlatitude or tropical regions, with the dominant process being the large wintertime cooling of the ocean surface during cold air outbreaks. Comparing the Q_s and Q_l time series, they are quite similar in character as they both depend on T_a and wind speed. The correlation coefficients, at 0.77 and 0.75, are much closer to that of T_a than to that of the wind speed. The regression slopes, at 0.82 and 0.84, are lower than that of T_a , a reflection of the model's underestimation of high winds and overestimation of low winds (Figure 3 and Table 1). The low regression slopes for Q_s and Q_l suggest the model time series may underestimate these components during periods of high heat flux. Overall, the comparison is good, and the means are within 5 W m^{-2} . For Q_r the comparison is generally very good, with $r = 0.97$ and a regression slope of 1.00. Overall, the correlation coefficient of Q_{tot} is 0.89, and the regression slope is 0.97, indicating that the AWS and model surface energy budgets compare very well. The bias in Q_{tot} is negligible (4 W m^{-2}). Despite

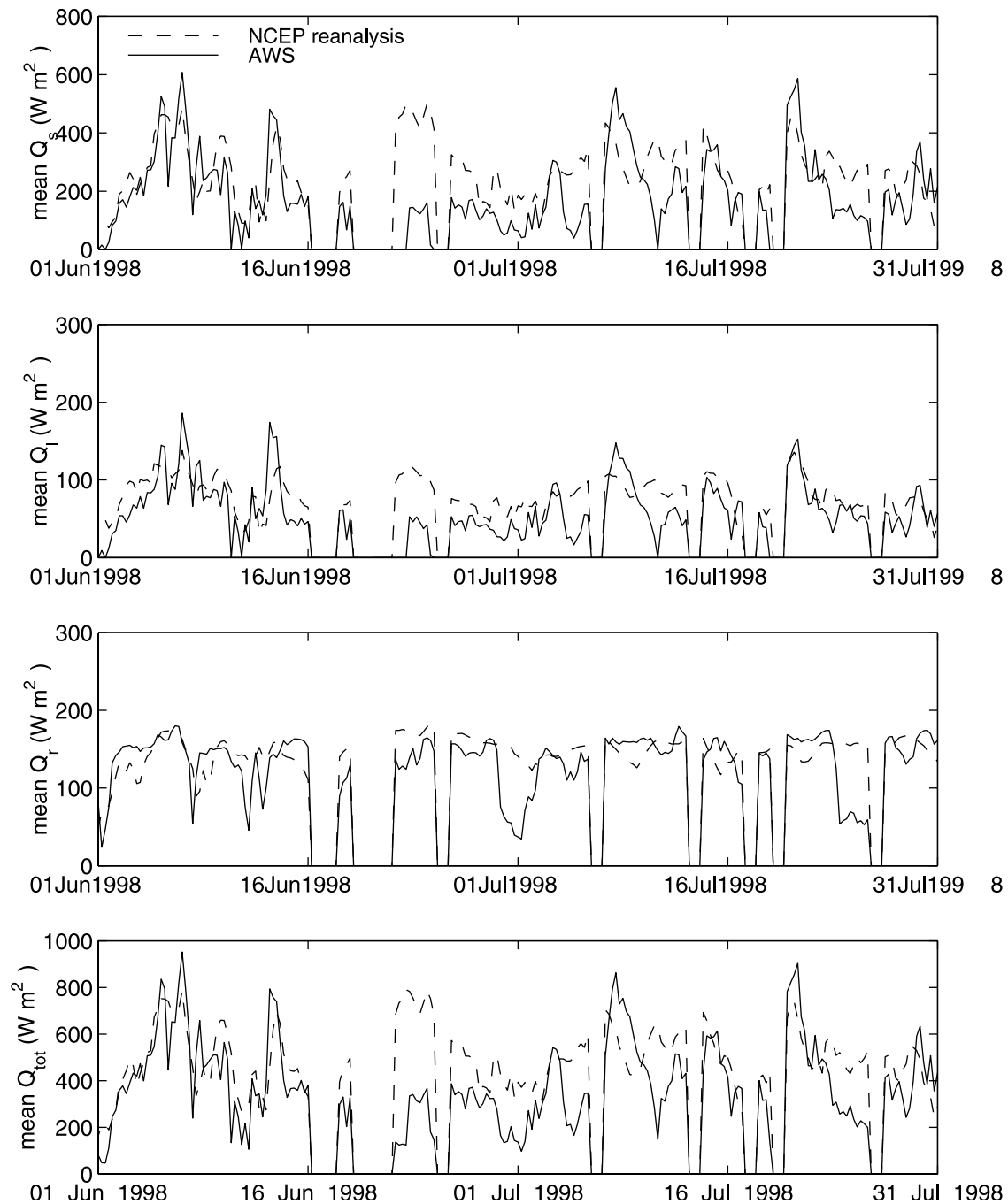


Figure 9. Time series from June-July 1998 showing the coastal polynya mean surface heat flux components (Q_s , Q_l , Q_r , and Q_{tot}) calculated via the NCEP reanalysis and the AWS time series as indicated.

the scatter in the comparison, overall, the comparison for Q_{tot} (and therefore ice production rates) is excellent. This gives us confidence that variability within the NCEP 7 year time series will be meaningful.

5. Variability of the Surface Energy Budget

[39] In this section we investigate the 7 year surface energy budget time series. Figure 10 plots the total surface heat flux (Q_{tot}) integrated over the coastal polynya area,

from (10). Each year alternates between a summer period of negative values, i.e., atmospheric cooling/oceanic warming, and a winter period of positive values, i.e., atmospheric warming/oceanic cooling. The winters are characterized by periods of positive fluxes, interspersed with quiescent periods when there is no polynya present, as seen in close up in Figure 9. The summer period also has considerable short-term variability, primarily from resolving the diurnal solar radiation signal. There are few summertime periods of zero flux, as there is usually

Table 4. A Comparison of Surface Heat Fluxes for 1 Year of Data From the AWS and Model (NCEP) Time Series^a

	$Q_{s, \text{AWS}}$ W m^{-2}	$Q_{s, \text{NCEP}}$ W m^{-2}	$Q_{s, \text{Model}}$ W m^{-2}	Q_{tot} W m^{-2}	Data Set
Mean	145.4	49.4	7.1	202.0	AWS
	149.9	50.5	-2.7	197.6	NCEP
Standard deviation	141.6	40.1	132.1	276.4	AWS
	150.7	44.8	135.8	303.8	NCEP
Maximum	865.8	223.9	198.8	1224.7	AWS
	791.6	175.0	182.6	1116.4	NCEP
Minimum	-21.6	-14.8	-354.6	-345.8	AWS
	-46.9	-34.5	-332.6	-368.3	NCEP
Correlation coefficient	0.77	0.75	0.97	0.89	AWS versus NCEP
Regression slope	0.82	0.84	1.00	0.97	AWS versus NCEP
Total rms error	206.7	60.1	189.6	410.6	AWS versus NCEP

^aThe fluxes are means averaged over the polynya area.

some open water present at this time. There is clearly some interannual variability in the time series, for example, some winters appear more active than others (i.e., more opening episodes), and there are tremendous differences between the summers: compare 1993–1994 to 1997–1998.

[40] The interannual variability is illustrated more clearly in Figure 11, which shows the cumulative area-integrated Q_{tot} (in Joules). This time series is initialized at zero on 1 January 1992. Since then there has been an overall oceanic warming due to the presence of coastal polynyas. On average the summertime oceanic energy gain outweighs the wintertime oceanic energy loss. To our knowledge this has not been established prior to this study. Previous

work has concentrated on the wintertime role of coastal polynyas as an oceanic heat sink and not investigated their summertime role as an oceanic heat source [e.g., *Cavaliere and Martin*, 1994; *Markus et al.*, 1998; *Comsio and Gordon*, 1998; *Winsor and Björk*, 2000]. The 7 year period of study is heavily influenced by the 1997–1998 summer season, which saw an anomalously large sea ice melt in the southern Weddell Sea [e.g., *Nicholls et al.*, 1998; *Ackley et al.*, 2001], leading to anomalous SWD absorption over a large area. If one considered (for example) the years 1992–1997, the summer oceanic warming and winter oceanic cooling appear closer to being in balance. It should be noted again here that these energy exchanges are integrations over coastal polynya area. This is only equivalent to an

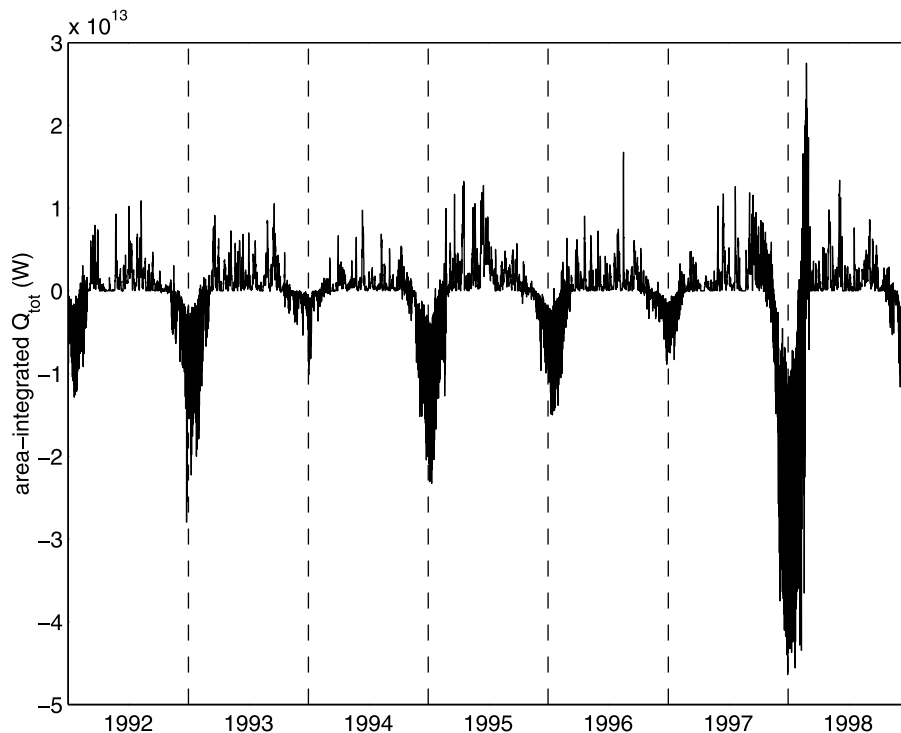


Figure 10. Seven year time series of area-integrated total surface heat flux. Positive values correspond to atmospheric warming (oceanic cooling), and negative values correspond to atmospheric cooling (oceanic warming).

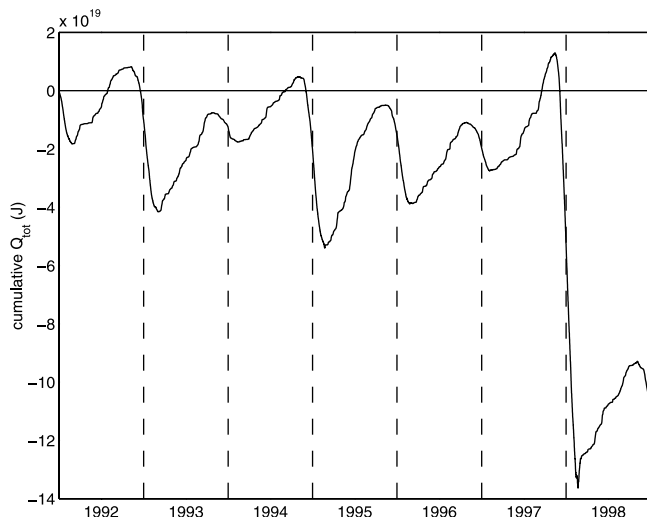


Figure 11. Seven year time series of cumulative area-integrated total surface heat flux for the coastal polynyas. A positive slope corresponds to the atmosphere's gaining energy (the ocean's losing energy). The freezing season is defined as the local minimum to the local maximum for each year.

integration over a constant domain if one assumes that there are no other heat exchanges, i.e., that the heat flux through the sea ice pack is zero and there are no horizontal heat fluxes. In reality, there are small fluxes through the ice pack and larger fluxes through leads within the ice pack. In addition, we know there are horizontal heat fluxes within the coastal ocean. However, quantifying these fluxes to a reasonable degree of accuracy is a study in itself; for example, what area of the pack ice is lead-covered at any one time? Therefore in this study we concentrate on accurate estimates of coastal polynya energy exchange and reserve the constant domain problem for further study.

[41] By plotting the cumulative area-integrated Q_{tot} the seasonal cycle is now well defined (Figure 11). We use this time series to define a freezing season (winter) and melting season (summer) for each year: the local minimum marks the start and the local maximum marks the end of the freezing season for each year. Using this definition, the

freezing season is the period that the ocean is losing energy to the atmosphere. Likewise, the melting season is defined as the local maximum in each year to the local minimum in the following year. These dates are noted in Tables 5 and 6. In any 1 year the largest oceanic energy loss is during the freezing season of 1995, with the 1998 and 1997 seasons also having above average energy losses. The dramatic oceanic energy gain during the melting season of 1997–1998 is the largest event of the time series and contrasts with some years of very little summertime energy gain (e.g., 1993–94 and 1996–1997).

[42] A closer examination of the surface energy budget and its components is presented in Figures 12 and 13 and summarized in Tables 5 and 6. For the freezing season, Figure 12a shows the cumulative coastal polynya area, Figure 12b shows cumulative Q_{tot} , Figure 12c shows cumulative Q_s , Figure 12d shows cumulative Q_l , and Figure 12e shows cumulative Q_r as a function of days into the freezing season. Figure 12a shows clearly the anomalous polynya of the 1997–1998 season. The rapid growth in cumulative polynya area starts around day 210 into the 1997 freezing season (around 4 September 1997) with a very active period of coastal polynya episodes and continues through the 1997–1998 melting season and into the following 1998 freezing season. It has been shown by *Ackley et al.* [2001] that this anomalous melt is coincident with anomalously strong offshore winds in spring 1997. These may be related to the strong El Niño event of the time, as there is some evidence that such events lead to anomalously low pressure in the Weddell Sea sector. After the large open water area freezes up, around day 15 of the 1998 freezing season, polynya activity is similar to previous years. Excepting 1998, the largest cumulative polynya area is in the 1995 freezing season. Figure 12 highlights again the episodic nature of coastal polynya ocean-atmosphere heat exchange. Here the spikes of high fluxes in Figures 9 and 10 correspond to rapid accumulations (steep gradients) in the Q terms. These are particularly ubiquitous in the Q_s and Q_l time series, reflecting the high fluxes induced by weather systems (e.g., Figures 2 and 6–9). The freezing season Q_{tot} time series are dominated by the Q_s components, with the Q_l and generally the Q_r components also contributing positively. Interestingly, the Q_s and Q_l series both closely resemble the cumulative polynya area series (Figure 12a). This is partly due to an

Table 5. Freezing Season Statistics: Showing Start and End Dates, Length of the Season, Cumulative Coastal Polynya Area, and Changes in the Coastal Polynya Surface Energy Budget and Components Over the Season^a

Year	Start	End	Length, days	Cumulative Polynya Area, $10^6 \text{ km}^2 \text{ days}$	ΣQ_{tot} , 10^{19} J	ΣQ_s , 10^{19} J	ΣQ_l , 10^{19} J	ΣQ_r , 10^{19} J
1992	26 February	9 November	256.5	0.68	2.65	1.65	0.52	0.47
1993	4 March	31 October	241.5	1.00	3.39	2.04	0.63	0.73
1994	15 February	1 November	258.5	0.83	2.25	1.38	0.45	0.41
1995	22 February	12 November	262.75	1.47	4.90	2.90	0.97	1.02
1996	25 February	27 October	244.75	1.03	2.80	1.67	0.56	0.56
1997	6 February	14 November	281.5	1.56	4.04	2.78	0.98	0.27
1998	21 February	5 November	256.75	2.28	4.35	2.90	1.34	0.09
Mean	20 February	5 November	257.5	1.26	3.48	2.19	0.78	0.51
Standard deviation	8.5 days	6.5 days	13	0.55	0.98	0.66	0.33	0.30

^a The annual mean and the standard deviation over the 7 years are also noted.

Table 6. Melting Season Statistics: Showing Start and End Dates, Length of the Season, Cumulative Coastal Polynya Area, and Changes in the Coastal Polynya Surface Energy Budget and Components Over the Season^a

Year	Start	End	Length, days	Cumulative Polynya Area, 10 ⁶ km ² days	ΣQ_{tot} , 10 ¹⁹ J	ΣQ_s , 10 ¹⁹ J	ΣQ_b , 10 ¹⁹ J	ΣQ_r , 10 ¹⁹ J
1992–1993	10 November	3 March	114.75	3.80	−4.97	0.09	0.09	−5.16
1993–1994	1 November	14 February	107.25	0.77	−1.00	0.04	0.03	−1.08
1994–1995	2 November	21 February	113.25	4.45	−5.88	0.12	0.12	−6.12
1995–1996	13 November	24 February	105.5	2.62	−3.39	0.06	0.06	−3.50
1996–1997	28 October	7 February	101.5	1.16	−1.66	0.05	0.04	−1.75
1997–1998	15 November	20 February	99.25	10.43	−14.93	−0.34	−0.10	−14.50
Mean	6 November	19 February	106.9	3.87	−5.31	0.004	0.04	−5.35
Standard deviation	6.5 days	8.5 days	6.1	3.52	5.07	0.16	0.07	4.88

^aThe annual mean and the standard deviation over the 6 years are also noted.

integration over the polynya area in calculating these time series but is perhaps also a reflection of all these series' dependence on the same variables: wind speed and temperature. Recall in Figure 2 we noted that the offshore wind speed is an important meteorological variable in determining coastal polynya area. Indeed, most theoretical polynya models use a linear relationship between near-surface wind speed and polynya width, with a strong dependency on air temperature and weaker dependencies on surface fluxes, ice type, ocean currents, and so on [e.g., Pease, 1987; Wilmott et al., 1997; Van Woert, 1999]. The standard bulk flux equations for Q_s and Q_l show the same: a linear dependence on wind speed and a strong dependence on temperature. The cumulative Q_r time series is generally positive, with the oceanic energy gains at the start and end of the freezing period due to SWD absorption in autumn and spring.

[43] Table 5 summarizes Figure 12 and some of the above discussion. The average freezing season total energy exchange (ΣQ_{tot}) is 3.48×10^{19} J, to which the Q_s , Q_b , and Q_r components contribute 63, 22, and 15%, respectively. It is clear that the greatest ΣQ_{tot} occurs in years with large polynya areas, but the relationship is not one to one. For example, a cold spell with a small polynya area could yield greater energy exchange than a warmer spell with a larger polynya area. The length of the freezing season does not appear to be related to the total energy exchanged. Although it should be noted that the interannual variability of the freezing season is quite small, the standard deviation is $\sim 5\%$ of the mean.

[44] For the melting season, Figure 13a shows the cumulative coastal polynya area and Figure 13b shows the cumulative Q_{tot} . The polynya area time series show a large range over the 6 seasons, with the greatest area occurring during the 1997–1998 season. Strictly speaking, the 1997–1998 meltback was so anomalous the region became open water rather than an enclosed polynya. By day 25 (10 December 1997) the region is entirely clear of sea ice (Figure 13a). Even excluding that year, the range from 0.77 to 4.45×10^6 km² days is substantial. The growth in open water area is less episodic during the melting season but is rather a combination of offshore wind events and a more gradual melting. The Q_{tot} time series are basically a mirror image of the polynya area series. The melting season surface energy budget is dominated by the absorption of SWD radiation in the Q_r term, with the Q_s and Q_l terms both an order of magnitude

smaller (Table 6). Hence the Q_{tot} time series is simply a reflection of the amount of low-albedo surface area available to absorb SWD radiation. As before, the length of the melting season does not appear to be related to the total energy exchanged.

[45] During the freezing season one can assume that a heat flux from the ocean to the atmosphere results directly in ice production, i.e., (10) holds assuming the ocean column is at freezing point. Hence the cumulative area-integrated Q_{tot} plotted in Figure 12b is proportional to the cumulative area-integrated ice production (in m³). This has been noted as a right-hand axis on Figure 12b. Viewed from this perspective, the episodic nature of ice production is emphasized, and consequently, the episodic nature of buoyancy forcing is emphasized. Following earlier comments, this suggests buoyancy forcing occurs on the timescales of coastal polynya dynamics, i.e., periods of days to weeks [see also Chapman, 1999]. Noting this point, we will proceed to examine the ice production time series by month, as well as by year. Although this does not entirely present an accurate picture of events (as active periods may bridge 2 months), it is a convenient time period to look at variability on a number of timescales.

[46] For the following time series, ice production is assumed if (1) $Q_{\text{tot}} > 0$ and (2) the data point lies within the freezing season. Note there are a few data points that lie outside the freezing season (as defined via Figure 12, see Table 5 for dates) where $Q_{\text{tot}} > 0$. At these times we assume the positive heat exchange leads to a cooling of the ocean rather than ice production. A simple calculation shows that the cooling of a 100 m deep column of water from -1.5°C to its freezing point can be achieved by only around 10 hours of 400 W m^{-2} surface cooling, consistent with the above assumptions. Figure 14 shows a bar chart of coastal polynya ice production per month. The results echo the freezing season Q_{tot} time series (Figure 12b) with 1995, 1998, and 1997 being the years of greatest ice production and 1994 the year of least ice production. Within each year there is a roughly normal distribution, modified by a great deal of month to month variability. The months of January and occasionally November and December have zero ice production. The highest ice production of any 1 month is around $4 \times 10^{10} \text{ m}^3$ in June 1995. The mean of all (March–October) months is $1.32 \times 10^{10} \text{ m}^3$.

[47] Figure 15 shows a month by month comparison of the coastal polynya ice production for 1998 as calculated

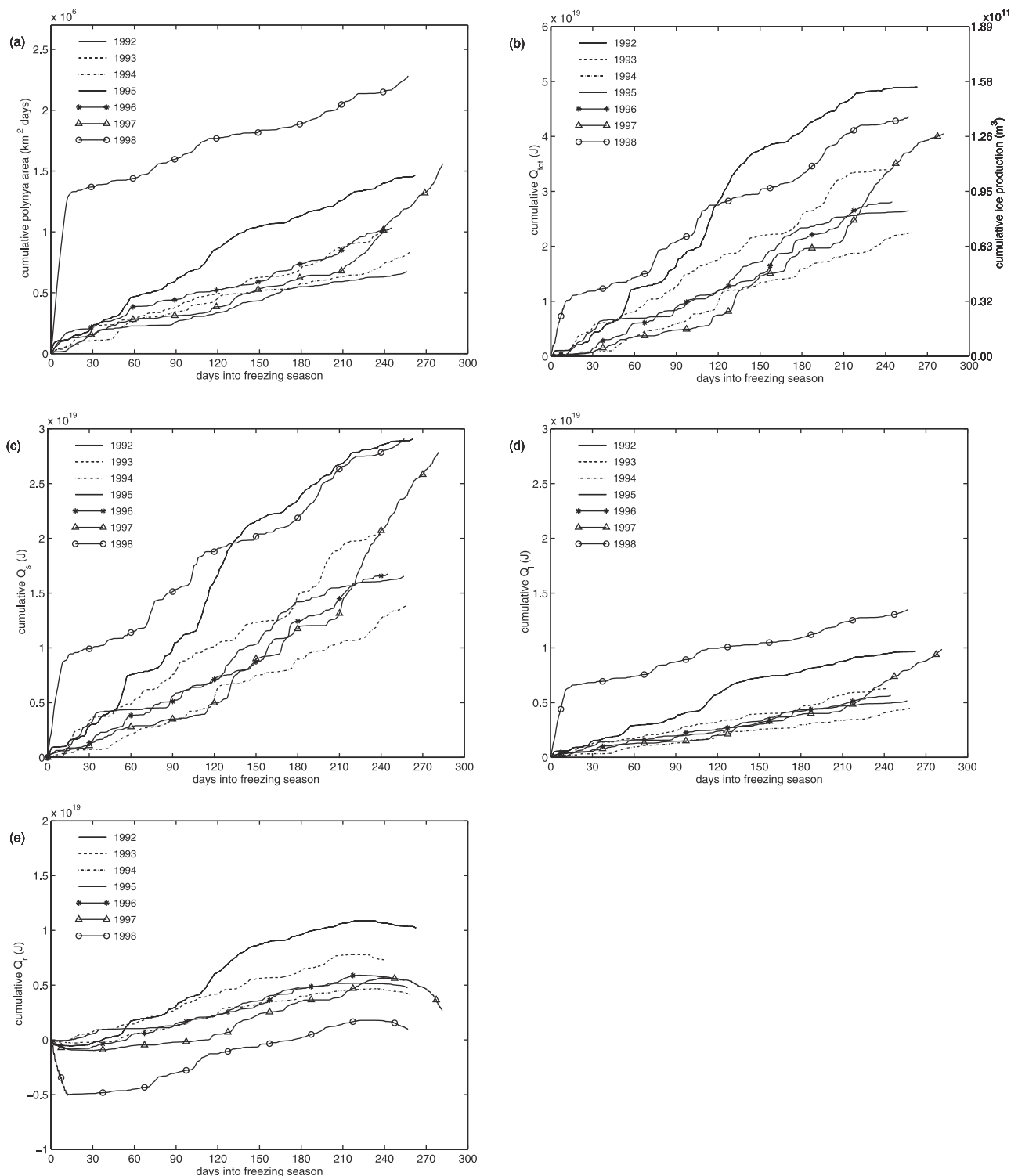


Figure 12. Multiyear time series of each freezing season: (a) cumulative polynya area, (b) cumulative (area-integrated) Q_{tot} , (c) cumulative Q_s , (d) cumulative Q_l , and (e) cumulative Q_r . The start and end dates of the freezing seasons are noted in Table 5.

using the AWS and NCEP time series (cf. section 4). In general, the correspondence is very good; the average difference between the monthly amounts is only 8%. The only substantial differences are in February and March, when remnants of the anomalous summertime melt-

back of 1997–1998 are still influencing the calculations (Figures 10, 11, 12a, and 13a). In general, during this period the NCEP model was too warm, too heavily influenced by the proximity of the grid point to the open water, so the model turbulent fluxes were too low. These relatively small

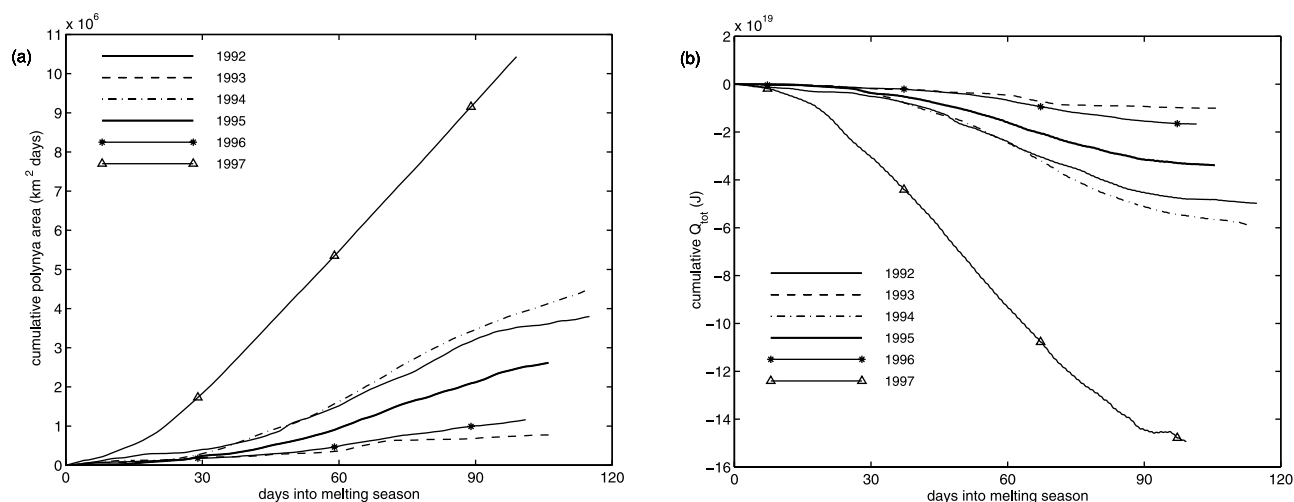


Figure 13. Multiyear time series of each melting season: (a) cumulative polynya area and (b) cumulative (area-integrated) Q_{tot} . The start and end dates of the melting seasons are noted in Table 6.

discrepancies in surface heat fluxes are magnified when integrated over the huge polynya area. If February and March were neglected, the difference in annual ice production between the two time series falls to below 2%. This comparison gives us great confidence in the fidelity of our 7 year time series and hence our ability to discern inter-annual variability.

[48] A number of annual ice production estimates are summarized in Table 7. The first column shows the average ice production per unit area of coastal polynya: the mean is 24.0 m, with a maximum of 31.7 m in 1992 and a minimum of 15.6 m in 1998. Note as these data are per unit area, in some sense they give a measure of the intensity of the freezing season. The fact that the range is large (a factor of 2) illustrates that the assumption of a constant heat flux (per unit area), as has been done in some surface energy

budget studies, is a very poor one. Indeed, it leads to surface heat flux estimates that at best are only accurate to within a factor of 2. The second column of Table 7 records the annual coastal polynya ice production for 1992–1998, equivalent to summing up over each year in Figure 14. The 7 year mean ice production is $1.11 \times 10^{11} \text{ m}^3$. The lowest and highest productions are 0.71×10^{11} and $1.55 \times 10^{11} \text{ m}^3$ in 1994 and 1995, respectively. The 1995 ice production is more than double that of the previous year! The interannual variability is large; the standard deviation of the 7 year time series is 28% of the mean value. Ranking the annual ice productions from highest to lowest yields 1995, 1998, 1997, 1993, 1996, 1992, and 1994. To place this in context, we have also examined the total sea ice production of the Weddell Sea (from 0 to 60°W). Passive microwave (SSM/I) data have been used to construct a daily time series

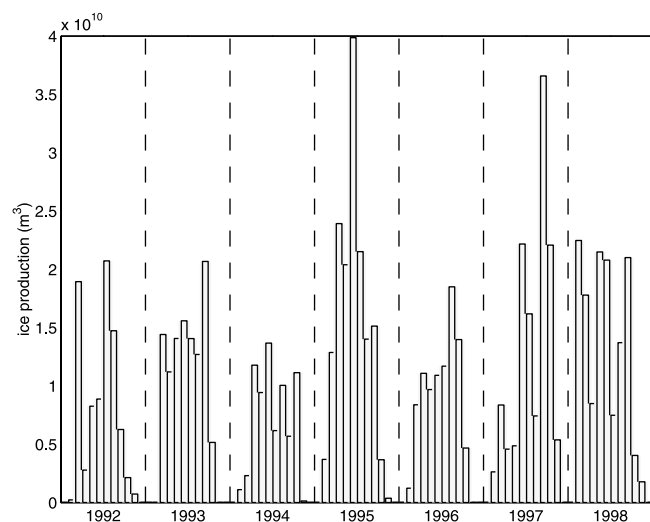


Figure 14. A bar chart of ice production (m^3) for each month of the 7 year climatology. Note there is zero ice production in January, and occasionally November and December of each years.

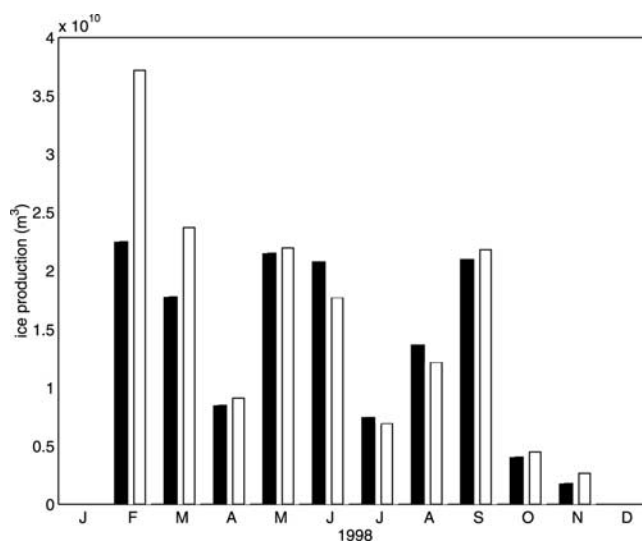


Figure 15. A bar chart of ice production amounts for each month of 1998 using the AWS (open bars) and NCEP (solid bars) meteorological time series as input to the calculation.

Table 7. Ice Production Amounts for Each Year of the Climatology, as well as the Mean and Standard Deviation of the 7 Years^a

	Coastal Polynya Average Ice Production, m	Coastal Polynya Ice Production, 10^{11} m^3	Weddell Sea Ice Production, 10^{11} m^3	Polynya Ice Production/ Weddell Sea Ice Production, %
1992	31.7	0.84	18.79	4.45
1993	26.1	1.08	17.60	6.13
1994	22.1	0.71	19.57	3.65
1995	27.7	1.55	17.07	9.11
1996	21.4	0.90	18.47	4.88
1997	23.5	1.30	17.86	7.29
1998	15.6	1.39	19.68	7.07
Mean	24.0	1.11	18.44	6.08
Standard deviation	5.1	0.31	0.99	1.90

^aThe columns show the average coastal polynya ice production (per unit area), the total coastal polynya ice production (calculated from the surface energy budget time series as described in the text), the total Weddell Sea ice production (assuming a mean ice thickness of 0.5 m), and the ratio of these last two amounts.

of sea ice extent and sea ice area (extent \times concentration) following, for example, *Cavaliere et al.* [1999]. To convert ice area into ice volume, one needs to assume an ice thickness. We assume an average sea ice thickness of 0.5 m [*Wadhams et al.*, 1987]. Clearly, if an average thickness of 1 m were used, the following ice production amounts would all be double that listed here. The third column in Table 7 records the Weddell Sea ice production. The 7 year mean is $18.44 \times 10^{11} \text{ m}^3$. The lowest and highest productions are 17.60×10^{11} and $19.68 \times 10^{11} \text{ m}^3$ in 1993 and 1998, respectively. The interannual variability in ice production is quite small; the standard deviation of the 7 year time series is only 5% of the mean value. This is in contrast to the interannual variability in the spatial distribution of sea ice, which is more substantial [*Comsio and Gordon*, 1998]. Ranking the Weddell Sea annual ice productions from highest to lowest yields 1998, 1994, 1992, 1996, 1997, 1993, and 1995. There does not appear to be any relationship between the annual coastal polynya ice production and the Weddell Sea ice production. On average the annual coastal polynya ice production is 6.08% of the total ice produced in the Weddell Sea, but this ratio varies from 3.65% in 1994 to 9.11% in 1995, the lowest and highest polynya ice production years.

[49] Both monthly and daily time series of Weddell Sea total ice extent and area have been examined (not shown). The annual cycle is clear, with minima typically in February and maxima typically in September of each year. The growth in sea ice through the autumn is steady, rather than episodic, with vacillations in area through the winter, before a steady ice pack retreat through the summer. There does not appear to be a direct link between periods of high coastal polynya ice production and periods of extensive Weddell Sea ice growth. Clearly, the 4–9% coastal polynya contribution to total ice volume is not large enough to control the variability of the entire Weddell Sea.

[50] These coastal polynya ice production estimates are somewhat higher than those of *Markus et al.* [1998]. Comparing our results with their Ronne-Filchner region (sector B) results, they find a mean ice production of $0.872 \times 10^{11} \text{ m}^3$ for the years 1992–1994 compared to our mean for these years $0.877 \times 10^{11} \text{ m}^3$. The agreement is somewhat misleading as their sector B is larger than our area of study as it includes the Filchner ice front. In

general, we calculate more ice production because of a generally colder atmospheric boundary layer. *Markus et al.* [1998] used the ECMWF analyses data for their study, which, as discussed in section 2, were biased warm during cold periods. They assumed this warm bias would be similar to the boundary layer modification seen as air flowed across the polynya. Our results using the CIBL model indicate that the boundary layer modification is more modest than this, and so overall, our sensible heat fluxes and thus our ice production are higher. *Markus et al.* studied a much larger area than we have, encompassing the entire coastline between 20°E and 60°W. They find coastal polynyas producing 2.5–5% of the total Weddell Sea ice volume (assuming ice thicknesses of 1–0.5 m, respectively). We examine just the most active area, the SW corner of the Weddell Sea, and find coastal polynyas producing 3.65–9.11% of the total ice produced depending on the year (assuming an ice thickness of 0.5 m). *Comsio and Gordon* [1998] also estimate coastal polynya area and salinization in the Weddell Sea region. They found generally greater polynya areas than *Markus et al.* [1998]. They use a simple relationship [from *Zwally et al.*, 1985] to relate changes in salinity to polynya area, length of winter, and a constant ice production rate. This is equivalent to assuming a constant heat flux into the atmosphere. As discussed above, the variability in sensible, latent, and radiative fluxes due to atmospheric variability suggests that this approach is an oversimplification of the problem.

6. Conclusions

[51] The surface energy budget of coastal polynyas in the southern Weddell Sea has been investigated through the combination of satellite observations, meteorological data, and simple physical models. The surface energy budget time series are illustrated through Figures 10–15 and Tables 4–7. For coastal polynyas in the freezing season, positive sensible heat fluxes dominate the surface energy budget, with latent and radiative heat fluxes generally augmenting the oceanic cooling. The turbulent heat fluxes are characterized by episodes of high heat fluxes, interspersed with more quiescent periods. Coastal polynya dynamics set the timescales for these changes: strong offshore winds blow open the

polynyas, which then refreeze at rates determined by the atmospheric and oceanic conditions. The total wintertime energy exchange is related to the cumulative coastal polynya area (indeed, the turbulent heat fluxes are strongly related); however, the varying atmospheric boundary layer is also important in modifying the fluxes. On average, the total energy exchange is 3.48×10^{19} J, with contributions of 63, 22, and 15% from the sensible, latent, and radiative terms, respectively. The wintertime energy exchange is not related to the length of the freezing season. For coastal polynyas in the melting season the area-integrated fluxes are dominated by the absorption of shortwave radiation. Over the 7 year period from 1992 to 1998 the ocean warms more than it cools through the presence of coastal polynyas. In particular, the anomalous summertime open water area of 1997–1998 allowed an enormous area-integrated warming of the ocean.

[52] During the freezing season, positive surface heat fluxes have been equated with ice production rates. The mean average coastal polynya ice production per unit area is 24.0 m, with a range from 15.6 (in 1998) to 31.7 m (in 1992). In terms of total annual coastal polynya ice production the mean is 1.11×10^{11} m³ with a range from 0.71×10^{11} (in 1994) to 1.55×10^{11} m³ (in 1995). The interannual variability is large: the standard deviation is 28% of the annual mean. Ice production has roughly a normal distribution over the freezing season, with strong modifications due to the episodic nature of the time series, for example, coastal polynya opening episodes may span a couple of months. These ice production calculations are compared to estimates of the ice production in the entire Weddell Sea from passive microwave data and an assumed average ice thickness of 0.5 m. The mean coastal polynya ice production is 6.08% of the entire Weddell Sea ice production, although this ratio varies from 3.65 (in 1994) to 9.11% (in 1995). The total annual Weddell Sea ice production does not vary that much: the standard deviation is only 5% of the mean. Hence variability in the ratio is determined primarily by changes in the coastal polynya ice production.

[53] An estimate of the accuracy of these results can be made through a comparison of the 1998 AWS and NCEP surface energy budgets. In the mean the components match remarkably well (to within 10 W m^{-2}). The correlation coefficients are over 0.75, and the linear regression slopes are over 0.8. The differences in mean monthly ice production are 8% over the whole year but only 2% if the anomalous months of February and March 1998 are ignored. This suggests that the use of the NCEP model data is well founded. For example, we would expect the time series to be accurate to within $\sim 5\%$ in terms of annual ice production. In addition to this however, there will be errors associated with (1) the determination of the sea ice cover, (2) the representativeness of the meteorological data, (3) the neglected physical processes in the CIBL model, and (4) the use of simple formulae for the radiative terms. We would estimate absolute errors associated with the above to be of the order 20%, in terms of the annual ice production, for example, but much less than that, of order 10%, when examining the interannual variability within the climatology. We are therefore confident that the interannual variability described here is genuine.

[54] A number of directions for future research have become apparent during this study. The transformation of

this surface energy budget into an oceanic buoyancy forcing is one objective of future work. To do this will involve the assessment of a number of physical processes that affect both the heat flux and, in particular, the freshwater flux, for example, precipitation, blowing snow deposition, ice shelf melt, and changes in the oceanographic conditions. The buoyancy forcing is a key ingredient for ongoing studies of sub-ice shelf oceanography and bottom water formation [Nicholls and Makinson, 1998; Comiso and Gordon, 1998], and so, a study along these lines is planned. The discovery of large interannual variability within the surface energy budget begs the question: what is causing it? We have noted earlier that coastal polynya dynamics are related to offshore winds and air temperature, among other things. Similarly, the surface energy budget is strongly related to wind speed and temperature through the turbulent heat flux terms. These variables are determined on the mesoscale and synoptic-scale by a variety of weather systems. Hence, for the southern Weddell Sea, variations in the synoptic-scale storm track [e.g., Simmonds and Keay, 2000; Marshall, 2000], in mesoscale cyclones [e.g., Heinemann, 1996; Turner et al., 1996], in barrier-forced winds [e.g., O'Connor et al., 1994], and in katabatic surges [e.g., Bromwich et al., 1992] will all play a role. At the moment, studies of atmospheric variability in this region are in their infancy. A detailed examination of coastal polynya forcing and its variability will be an essential step toward understanding the atmosphere-ocean-ice system of this region.

[55] **Acknowledgments.** The NCEP/NCAR reanalyses data were provided by NOAA Climate Diagnostics Center. We would like to thank R. Grumbine (NOAA) for his help with deciphering the sea ice cover used in the NCEP/NCAR reanalyses and Steve Leonard for help reading the model data. Data from AWS “Limbart” were provided by the Antarctic Meteorological Research Center at the University of Wisconsin as part of the U.S. Antarctic Automatic Weather Station Project, which is supported by the National Science Foundation. This study has benefited from discussions with Keith Nicholls.

References

- Ackley, S. F., C. Geiger, J. C. King, E. C. Hunke, and J. Comiso, The Ronne Polynya of 1997–98: Observations of air-ice-ocean interaction, *Ann. Glaciol.*, **33**, 425–429, 2001.
- Alam, A., and J. A. Curry, Evolution of new ice and turbulent fluxes over freezing winter leads, *J. Geophys. Res.*, **103**, 15,783–15,802, 1998.
- Andreas, E. L., and B. Murphy, Bulk transfer coefficients for heat and momentum over leads and polynyas, *J. Phys. Oceanogr.*, **108**, 1875–1883, 1986.
- Bromwich, D. H., J. F. Carrasco, and C. R. Stearns, Satellite observations of katabatic-wind propagation for great distances across the Ross Ice Shelf, *Mon. Weather Rev.*, **120**, 1940–1949, 1992.
- Bromwich, D. H., R. I. Cullather, and R. W. Grumbine, An assessment of the NCEP operational global spectral model and analyses for Antarctica during FROST, *Weather Forecasting*, **14**, 835–850, 1999.
- Brümmer, B., Boundary layer mass, water and heat budgets in wintertime cold-air outbreaks from the arctic sea ice, *Mon. Weather Rev.*, **125**, 1824–1837, 1997.
- Cavaliere, D. J., and S. Martin, The contribution of Alaskan, Siberian, and Canadian coastal polynyas to the cold halocline layer of the Arctic Ocean, *J. Geophys. Res.*, **99**, 18,343–18,362, 1994.
- Cavaliere, D. J., C. L. Parkinson, P. Gloersen, J. C. Comiso, and H. J. Zwally, Deriving long-term time series of sea ice cover from satellite passive-microwave multisensor data sets, *J. Geophys. Res.*, **104**, 15,803–15,814, 1999.
- Chang, S. S., and R. R. Braham, Observational study of a convective internal boundary layer over Lake Michigan, *J. Atmos. Sci.*, **48**, 2265–2279, 1991.
- Chapman, D. C., Dense water formation beneath a time-dependent coastal polynya, *J. Phys. Oceanogr.*, **29**, 807–820, 1999.

- Comsio, J. C., and A. L. Gordon, Interannual variability in summer sea ice minimum, coastal polynyas and bottom water formation in the Weddell Sea, in *Antarctic Sea Ice: Physical Processes, Interaction, and Variability*, *Antartarct. Res. Ser.* vol. 74, edited by M. O. Jeffries, pp. 293–315, AGU, Washington, D. C., 1998.
- Curry, J. A., and P. J. Webster, *Thermodynamics of Atmospheres and Oceans*, 471 pp., Academic, San Diego, Calif., 1999.
- Dare, R. A., and B. W. Atkinson, Numerical modeling of atmospheric response to polynyas in the Southern Ocean sea ice zone, *J. Geophys. Res.*, 104, 16,691–16,708, 1999.
- DeCosmo, J., K. B. Katsaros, S. D. Smith, R. J. Anderson, W. A. Oost, K. Bumke, and H. Chadwick, Air-sea exchange of water vapor and sensible heat: The Humidity Exchange Over the Sea (HEXOS) results, *J. Geophys. Res.*, 101, 12,001–12,016, 1996.
- Foldvik, A., and T. Gammelsrød, Notes on Southern Ocean hydrography, sea ice and bottom water formation, *Palaeogeogr. Palaeoclimatol. Palaeoecol.*, 67, 3–17, 1988.
- Gamo, M., S. Yamamoto, O. Yokoyama, and H. Yashikado, Structure of the free convective internal boundary layer during the sea breeze, *J. Meteorol. Soc. Jpn.*, 61, 1284–1298, 1983.
- Garratt, J. R., *The Atmospheric Boundary Layer*, Cambridge Univ. Press, 316 pp., New York, 1992.
- Grossman, R. L., and A. K. Betts, Air-sea interaction during an extreme cold air outbreak from the eastern coast of the United States, *Mon. Weather Rev.*, 118, 324–342, 1990.
- Heinemann, G., On the structure and energy budget of the boundary layer in the vicinity of the Filchner/Ronne Ice Shelf front (Antarctica), *Beitr. Phys. Atmos.*, 61, 244–258, 1988.
- Heinemann, G., On the development of wintertime meso-scale cyclones near the sea ice front in the Arctic and Antarctic, *Global Atmos. Ocean System*, 4, 89–124, 1996.
- Hines, K. M., R. W. Grumbine, D. H. Bromwich, and R. I. Cullather, Surface energy balance of the NCEP MRF and NCEP-NCAR reanalyses in Antarctic latitudes during FROST, *Weather Forecasting*, 14, 851–866, 1999.
- Hines, K. M., D. H. Bromwich, and G. J. Marshall, Artificial surface pressure trends in the NCEP/NCAR reanalyses over the Southern Ocean and Antarctica, *J. Clim.*, 13, 3940–3952, 2000.
- Kalnay, E., et al., The NCEP/NCAR 40-year reanalysis project, *Bull. Am. Meteorol. Soc.*, 77, 437–471, 1996.
- Key, J., and A. J. Schweiger, Tools for atmospheric radiative transfer: Streamer and fluxnet, *Comput. Geosci.*, 24, 443–451, 1998.
- Killworth, P. D., Deep convection in the world ocean, *Rev. Geophys.*, 21, 1–26, 1983.
- King, J. C., Some measurements of turbulence over an antarctic ice shelf, *Q. J. R. Meteorol. Soc.*, 116, 379–400, 1990.
- King, J. C., and P. S. Anderson, A humidity climatology for Halley, Antarctica, based on frost-point hygrometer measurements, *Antarct. Sci.*, 11, 100–104, 1999.
- King, J. C., M. J. Varley, and T. A. Lachlan-Cope, Using satellite thermal infrared imagery to study boundary layer structure in an Antarctic katabatic wind region, *Int. J. Remote Sens.*, 19, 3335–3348, 1998.
- König-Langlo, G., and E. Augstein, Parameterization of the downward long-wave radiation at the Earth's surface in polar regions, *Meteorol. Z.*, 3, 343–347, 1994.
- Makshtas, A. P., E. L. Andreas, P. N. Svyashchennikov, and V. F. Timachev, Accounting for clouds in sea ice models, *Atmos. Res.*, 52, 77–113, 1999.
- Markus, T., and B. A. Burns, A method to estimate subpixel-scale coastal polynyas with satellite passive microwave data, *J. Geophys. Res.*, 100, 4473–4487, 1995.
- Markus, T., C. Kottmeier, and E. Fahrbach, Ice formation in coastal polynyas in the Weddell Sea and their impact on oceanic salinity, in *Antarctic Sea Ice: Physical processes, interaction, and variability*, *Antarct. Res. Ser.*, vol. 74, edited by M. O. Jeffries, pp. 273–292, AGU, Washington, D. C., 1998.
- Marshall, G. J., An examination of the precipitation regime at Thurston Island, Antarctica, from ECMWF re-analysis data, *Int. J. Climatol.*, 20, 255–277, 2000.
- Martin, S., R. Drucker, and K. Yamashita, The production of ice and dense shelf water in the Okhotsk Sea polynyas, *J. Geophys. Res.*, 103, 27,771–27,782, 1998.
- McPhee, M. G., and D. G. Martinson, Turbulent mixing under drifting pack ice in the Weddell Sea, *Science*, 263, 218–221, 1994.
- Moore, G. W. K., K. Alverson, and I. A. Renfrew, A reconstruction of the air-sea interaction associated with the Weddell Polynya, *J. Phys. Oceanogr.*, 32, 1685–1698, 2002.
- Nicholls, K. W., and K. Makinson, Ocean circulation beneath the western Ronne Ice Shelf, as derived from in situ measurements of water currents and properties, in *Ocean, Ice, and Atmosphere: Interactions at the Antarctic Continental Margin*, *Antarct. Res. Ser.*, vol. 75, edited by S. S. Jacobs and R. F. Weiss, pp. 301–318, AGU, Washington, D. C., 1998.
- Nicholls, K., S. Ackley, E. Hunke, B. Moat, and R. Woodgate, Cruise report for ROPEX 1997/98, *Br. Antarct. Surv. Int. Rep. GEN/1997/S2*, 30 pp., Cambridge, UK, 1998.
- O'Connor, W. P., D. H. Bromwich, and J. F. Carrasco, Cyclonically forced barrier winds along the Transantarctic Mountains near Ross Island, *Mon. Weather Rev.*, 122, 137–150, 1994.
- Pease, C. H., The size of wind-driven coastal polynyas, *J. Geophys. Res.*, 92, 7049–7059, 1987.
- Reed, R. K., On estimating insolation over the ocean, *J. Phys. Oceanogr.*, 7, 482–485, 1977.
- Renfrew, I. A., and J. C. King, A simple model of the convective internal boundary layer and its application to surface heat flux estimates within polynyas, *Boundary Layer Meteorol.*, 94, 335–356, 2000.
- Renfrew, I. A., and G. W. K. Moore, An extreme cold-air outbreak over the Labrador Sea: Roll vortices and air-sea interaction, *Mon. Weather Rev.*, 127, 2379–2394, 1999.
- Renfrew, I. A., G. W. K. Moore, P. S. Guest, and K. Bumke, A comparison of surface-layer and surface turbulent-flux observations over the Labrador Sea with ECMWF analyses and NCEP reanalyses, *J. Phys. Oceanogr.*, 32, 383–400, 2002.
- Simmonds, I., and K. Keay, Variability of Southern Hemisphere extratropical cyclone behaviour, 1958–97, *J. Clim.*, 13, 550–561, 2000.
- Smith, S. D., Coefficients for sea surface wind stress, heat flux, and wind profiles as a function of wind speed and temperature, *J. Geophys. Res.*, 93, 15,467–15,472, 1988.
- Smith, S. D., R. D. Muench, and C. H. Pease, Polynyas and leads: An overview of physical processes and environment, *J. Geophys. Res.*, 95, 9461–9479, 1990.
- Stearns, C. R., L. M. Keller, G. A. Weidner, and M. Sievers, Monthly mean climatic data for Antarctic automatic weather stations, in *Antarctic Meteorology and Climatology: Studies Based on Automatic Weather Stations*, *Antarct. Res. Ser.*, vol. 61, edited by D. H. Bromwich and C. R. Stearns, pp. 1–21, AGU, Washington, D. C., 1993.
- Stunder, M., and S. SethuRaman, A comparative evaluation of the coastal internal boundary-layer height equations, *Boundary Layer Meteorol.*, 32, 177–204, 1995.
- Turner, J., G. Corcoran, S. Cummins, T. Lachlan-Cope, and S. Leonard, Seasonal variability of mesocyclone activity in the Bellingshausen/Weddell region of Antarctica, *Global Atmos. Ocean System*, 5, 73–97, 1996.
- Turner, J., S. Leonard, G. J. Marshall, L. Cowled, R. Jardine, S. Pendlebury, and N. Adams, An assessment of operational Antarctic analysis based on data from the FROST project, *Weather Forecasting*, 14, 817–834, 1999.
- Van Woert, M., Wintertime dynamics of the Terra Nova Bay polynya, *J. Geophys. Res.*, 104, 7753–7769, 1999.
- Venkatram, A., A model of internal boundary-layer development, *Boundary Layer Meteorol.*, 11, 419–437, 1977.
- Wadhams, P., M. A. Lange, and S. F. Ackley, The ice thickness distribution across the Atlantic sector of the Antarctic Ocean in midwinter, *J. Geophys. Res.*, 92, 14,535–14,552, 1987.
- Wilmott, A. J., M. A. Morales Maqueda, and M. S. Darby, A model for the influence of wind and oceanic currents on the size of a steady-state latent heat coastal polynya, *J. Phys. Oceanogr.*, 27, 2256–2275, 1997.
- Winsor, P., and G. Björk, Polynya activity in the Arctic Ocean 1958–1997, *J. Geophys. Res.*, 105, 8789–8803, 2000.
- Zillman, J. W., A study of some aspects of the radiation and heat budgets of the Southern Hemisphere oceans, in *Meteorological Studies*, vol. 26, 562 pp., Bur. of Meteorol., Dep. of the Inter. Canberra, Australia, 1972.
- Zwally, H. J., J. C. Comiso, and A. Gordon, Antarctic offshore leads and polynyas and oceanographic effects, in *Oceanology of the Antarctic Continental Shelf*, *Antarct. Res. Ser.*, vol. 43, pp. 203–226, AGU, Washington, D. C., 1985.

J. C. King and I. A. Renfrew, British Antarctic Survey, High Cross, Madingley Road, Cambridge CB3 0ET, UK. (i.renfrew@bas.ac.uk)
T. Markus, NASA Goddard Space Flight Center, Greenbelt, MD USA.